



**Daniel Alfredo de Sá Pereira**

Licenciado em Ciências de Engenharia de Micro e Nanotecnologias

**Control of a White Organic Light Emitting Diode's emission parameters using a single doped RGB active layer**

Dissertação para obtenção do Grau de Mestre em Engenharia de Micro e Nanotecnologias

Orientador: Professor Doutor Luiz Fernando Ribeiro Pereira, Professor Auxiliar,  
Departamento de Física, Universidade de Aveiro

Co-orientador: Professora Doutora Isabel Maria das Mercês Ferreira,  
Professora Associada, Departamento das Ciências dos Materiais, Faculdade  
de Ciências e Tecnologias da Universidade Nova de Lisboa

**Júri:**

**Presidente: Prof. Doutor Rodrigo Martins**

**Arguente: Prof. Doutor Henrique Gomes**

**Vogal: Prof. Doutor Luiz Pereira**



FACULDADE DE  
CIÊNCIAS E TECNOLOGIA  
UNIVERSIDADE NOVA DE LISBOA

September 2015



*“There is a single light of science,  
and to brighten in anywhere is to brighten it everywhere.”*

– Isaac Asimov



**Control of a White Organic Light Emitting Diode's emission parameters using a single doped RGB layer**

Copyright © Daniel Alfredo de Sá Pereira, 2015.

A Faculdade de Ciências e Tecnologia e a Universidade Nova de Lisboa tem o direito, perpétuo e sem limites geográficos, de arquivar e publicar esta dissertação através de exemplares impressos reproduzidos em papel ou de forma digital, ou por qualquer outro meio conhecido ou que venha a ser inventado, e de a divulgar através de repositórios científicos e de admitir a sua cópia e distribuição com objetivos educacionais ou de investigação, não comerciais, desde que seja dado crédito ao autor e editor.



## **Acknowledgements**

Todas as pessoas aqui presentes fizeram, de certa forma, a diferença ao longo destes 5 anos de percurso académico e merecem uma especial menção. Queria agradecer, desde já, a todos os que lá estiveram, nos bons e maus momentos e que, de alguma forma contribuíram para que este momento chegasse.

Gostaria de começar por agradecer ao meu orientador, o Professor Dr. Luiz Pereira, que me recebeu e orientou na Universidade de Aveiro e cujo apoio, dedicação e entusiasmo pela área fizeram toda a diferença ao longo dos vários momentos que constituíram esta fase. Um grande obrigado por tudo. À minha orientadora da FCT-UNL, Prof. Dra. Isabel Ferreira, que me abriu bastantes portas e foi uma grande ajuda nestes últimos anos.

Aos meus pais, Rui e Esmeralda, a quem dedico esta tese, por 23 anos de uma formidável compreensão. Se sou o que sou e se cheguei onde cheguei a vocês o devo e meras palavras não chegam para descrever o meu agradecimento.

À minha irmã Vera que me ensinou que, se fizermos o que gostamos, não temos que trabalhar um único dia nas nossas vidas, ao Ariel, que se conseguir ler isto em português significa que já faz parte da família e ao meu primo Ricardo, que facilmente se tornou um suporte nesta família.

Aos meus tios, António e Irene e aos seus fantásticos filhos Filipa, Bruno e Mariana pelos vários anos de momentos perfeitos.

Ao Engenheiro João Gomes que me recebeu no CeNTI e ao André Pinto pelo apoio na construção dos OLEDs de larga área, um muito obrigado.

A todas as pessoas do Departamento de Física da Universidade de Aveiro que me ajudaram na transição e me receberam como um deles em especial ao Cláudio e à Rosa pela ajuda nas medições de PL e de PLE das minhas amostras.

A special thank you to Dr. Stefan Nowy for the help provided in the Impedance Spectroscopy analysis.

Ao Prof. Dr. Rodrigo Martins e à Prof. Dra. Elvira Fortunato pela criação, promoção e reconhecimento alcançado pelo curso de Engenharia Micro e Nanotecnologias.

À Sónia e à Sara da secretaria do Departamento de Materiais que foram sempre impecáveis quando eu precisei, um muito obrigado.

À Farah, não é preciso dizer nada mas obrigado por todas as conversas, idas aleatórias a Lisboa, interails, passeios e uma amizade como nunca julguei ser possível ter. Estes 5 anos, sem ti, não teriam sido a mesma coisa e apesar de já não sermos praticamente vizinhos, sinto que estamos mais próximos que nunca. O que são uns países entre nós? À Catarina, parceira dos trabalhos, dos projectos, do estudo mas acima de tudo parceira de imensos cafés, idas ao ginásio, chamadas internacionais e uma amizade incondicional. Ao Emanuel, um óptimo grande amigo, ensinaste-me que se dermos um pouco mais de nós, conseguimos chegar lá, acima de tudo em equipa.

Ao João Jacinto, foste a primeira pessoa com quem falei na FCT e 5 anos depois, só tenho a agradecer todo a ajuda, todas as conversas e conselhos e aquele verão fantástico com o pessoal.

Ao Panda Alex, que me ensinou que existe uma dinâmica fora do normal (mas muito especial) na infindável quantidade de cafés que se pode beber com uma pessoa. Está prometida a ida ao Sansouci!!!! À Joana, que tinha razão no que disse sobre Berlim e sobre o voltar de Berlim. À Rita Pontes pelas dormidas, idas a bares no meio de Almada, cornetos de morango e ajuda em

pitchos e à Teresa Kullberg que me ensinou que existe muito que se lhe diga na conceção de um pudim de pós. Ao Zé Rui, porque há muito que se lhe diga numa sessão de magia (claro que te tinha que associar a isto).

Ao André Abreu, obrigado por estares sempre do meu lado e pelos jantares, cinemas, idas a Lisboa, gelados,... (ainda me deves a visita a Aveiro). Não me esqueço claro da parceira do GIM, Maggie, e do Samuel e do Hugo.

Aos grandes Júlio Costa (irmão iNOVO), Nuno Coelho (epa quase que transmito sentimentos aqui) e Diogo Vaz (*Penus Orniturrincus*) pelas noites aleatórias nesse grande Basolho. Às melhores afilhadas do mundo, Joana (diversos cremes nas costas), Sofia (diversos momentos de descontração) e Constança (diversas conversas sobre séries e viagens pela Alemanha), a vocês todos uma palavra chega: ÇIM!

Ao Ricardo, a viagem à Islândia ainda está por realizar e ao Serafim pelos mais variados conselhos nestes últimos anos.

To my fantastic HZB family, Paula, Gianluca, Andrea, Juanita, Omar, Jennifer, Zack, Arturo, Marina and Guillermo I'll never forget you and I know that, in the future we will be all together again. You easily became a part of my everyday life so for that I thank you.

À minha recém contratada nutricionista Juliana e aos restantes Aneuréticos, Daniela, Miguel, Zé, Carla, Joana, Alex, Jorge, Silvinha um grande grupo de pessoas.

Ao Diogo Almeida por ter sido uma presença tão importante na minha estadia em Aveiro, seja pela companhia, seja pelas viagens e concertos por esse país fora. To Paulo Laranjeira, because it makes perfect sense to write this in English, for the Tuesdays and Thursdays (and other days) lunch hours. Oh, and for the Kikis.

A todas as pessoas do curso de MIEMN, aos que frequentam a 202 e a todos os que, de alguma forma, contribuíram para que me tornasse na pessoa que sou hoje e que não foram mencionados em cima.







## **Abstract**

White Color tuning is an attractive feature that Organic Light Emitting Diodes (OLEDs) offer. Up until now, there hasn't been any report that mix both color tuning abilities with device stability. In this work, White OLEDs (W-OLEDs) based on a single RGB blend composed of a blue emitting N,N'-Di(1-naphthyl)-N,N'-diphenyl-(1,1'-biphenyl)-4,4'-diamine (NPB) doped with a green emitting Coumarin-153 and a red emitting 4-(Dicyanomethylene)-2-methyl-6-(4-dimethylaminostyryl)-4H-pyran (DCM1) dyes were produced. The final device structure was ITO/Blend/Bathocuproine (BCP)/Tris(8-hydroxyquinolato)aluminium (Alq<sub>3</sub>)/Al with an emission area of 0.25 cm<sup>2</sup>. The effects of the changing in DCM1's concentration (from 0.5% to 1% wt.) allowed a tuning in the final white color resulting in devices capable of emitting a wide range of tunes – from cool to warm – while also keeping a low device complexity and a high stability. Moreover, an explanation on the optoelectrical behavior of the device is presented. The best electroluminescence (EL) points toward 160 cd/m<sup>2</sup> of brightness and 1.1 cd/A of efficiency, both prompted to being enhanced. An Impedance Spectroscopy (IS) analysis allowed to study both the effects of BCP as a Hole Blocking Layer and as an aging probe of the device. Finally, as a proof of concept, the emission was increased 9 and 64 times proving this structure can be effectively applied for general lighting.

**Keywords:** White OLED, Emission Color tuning, Blend EML, Host:Guest, Color Stability, Large Area



## **Resumo**

Um dos maiores fatores de atratividade dos Díodos Orgânicos Emissores de Luz (OLEDs) é a capacidade de tonalizar a cor final a ser emitida. Até aqui, não foram apresentados estudos que misturassem essa capacidade com a estabilidade dos dispositivos. Neste trabalho, foram fabricados OLEDs Brancos (W-OLEDs) baseados numa camada emissora RGB composta por uma blenda de N,N'-Di(1-naphthyl)-N,N'-diphenyl-(1,1'-biphenyl)-4,4'-diamine (NPB) dopado com um emissor verde, Coumarin-153 e um emissor vermelho, 4-(Dicyanomethylene)-2-methyl-6-(4-dimethylaminostyryl)-4H-pyran (DCM1). A estrutura final de cada dispositivo foi ITO/Blenda/ Bathocuproine (BCP)/Tris(8-hydroxyquinolato)aluminium (Alq<sub>3</sub>)/Al para uma emissão de 0.25 cm<sup>2</sup>. Ao variar a concentração de DCM1 (de 0.5 para 1% wt.), foi possível ajustar a cor branca resultando em dispositivos capazes de emitir uma grande gama de tons – do branco frio ao branco quente – a uma estrutura simples e uma estabilidade alta. Além disso, é feita uma explicação ao mecanismo responsável por este comportamento. Os melhores resultados de electroluminescência (EL) apontam para um brilho de 160 cd/m<sup>2</sup> e uma eficiência de 1.1 cd/A, ambos alvos de possíveis melhorias. Um estudo de Espectroscopia de Impedância (IS) foi também realizado para, não só avaliar a capacidade retentora de buracos do BCP, como também uma prova de envelhecimento a que os dispositivos são alvo. Finalmente, como prova de conceito, a emissão foi aumentada em 9 e 64 vezes mostrando, assim a aplicabilidade desta estrutura para iluminação.

**Palavras-chave:** OLED branco, Ajuste de cor, Estabilidade de cor, Blenda RGB, *Host:Guest*, Larga Área



## **Abbreviations**

CCT	Correlated Color Temperature
CFL	Compact Fluorescent Lamp
CIE	Commission Internationale de L'éclairage
CRI	Color Rendering Index
C153	Coumarin-153
CV	Capacitance-Voltage
EBL	Electron Blocking Layer
EEW	Equal Energy White
EIL	Electron Injection Layer
EL	Electroluminescence
EML	Electroluminescence Layer
ETL	Electron Transport Layer
HOMO	Highest Occupied Molecular Orbital
HBL	Hole Transport Layer
HIL	Hole Injection Layer
HTL	Hole Transport Layer
ITO	Indium Tin Oxide
IS	Impedance Spectroscopy
LED	Light Emitting Diode
LUMO	Lowest Unoccupied Molecular Orbital
OLED	Organic Light Emitting Diode
PL	Photoluminescence
PLE	Photoluminescence Excitation
PLED	Polymer Light Emitting Diode
RGB	Red Green Blue
RISC	Reverse Intersystem Crossing
R2R	Roll-to-Roll
SCLC	Space Charge Limited Current
SSL	Solid State Lighting
TADF	Thermally Activated Delayed Fluorescence
UV	Ultraviolet





## Symbols

min	minute	
$V_{TFL}$	Trap Fill Limit Voltage	V
$V_t$	Threshold Voltage	V
$V_{\Omega}$	Ohmic regime limit voltage	V
$V_{bi}$	Built-in Potential	V
$E_g$	Energy Gap	eV
$E_0$	Vacuum level	eV
$S_n$	Singlet energy level	( $n=0$ – fundamental state, $n=1,2,3,\dots$ – excited states)
$T_n$	Triplet energy level	( $n=1,2,3,\dots$ – excited states)
$h$	Planck constant	$6.626 \cdot 10^{-34}$ m <sup>2</sup> .kg/s
$\lambda$	Wavelength	nm
wt%	Weight percentage	
$\epsilon_r$	Dielectric constant	F·m <sup>-1</sup>
$\epsilon_0$	Vacuum permittivity constant	$8.854 \cdot 10^{-12}$ F·m <sup>-1</sup>



## **Table of Contents**

Acknowledgements .....	vii
Abstract .....	xi
Resumo .....	xiii
Abbreviations.....	xv
Symbols.....	xvii
Table of Contents .....	xix
List of Figures .....	xxi
List of Tables .....	xxv
Objective.....	1
Work structure .....	1
Motivation .....	3
1. Towards OLED lighting .....	3
2. The circadian rhythm.....	3
Chapter I: Introduction.....	5
1. Organic Light Emitting Diode's operation.....	5
<b>1.1. Hybridization in Organic Semiconductors</b> .....	5
<b>1.2. Charge Transport</b> .....	6
<b>1.2.1. The Hopping process</b> .....	6
<b>1.2.2. Space Charge Limited Current</b> .....	7
<b>1.3. Light Generation: Fluorescence and Phosphorescence</b> .....	8
2. W-OLEDs for Solid State Lighting .....	9
<b>2.1. Selective doping – the Host:Guest System</b> .....	10
Chapter II: Materials and Structure .....	13
Chapter III: Experimental.....	15
1. Substrate and Sample Preparation .....	15
2. Films Deposition .....	15
3. Device Characterization .....	16
Chapter IV: Results and Discussion.....	17

1. Blend Definition .....	17
2. Device Dynamics.....	18
<b>2.1. Electroluminescence Spectra and Figures of Merit</b> .....	18
<b>2.2. Device Stability</b> .....	19
<b>2.3. Photophysical and energy level analysis: operation theory</b> .....	20
3. Optoelectronic Characterization .....	23
4. a.c. analysis.....	26
<b>4.1. Impedance Spectroscopy (IS)</b> .....	26
<b>4.2. Capacitance-Voltage</b> .....	28
<b>4.3. Aging Studies</b> .....	29
5. Large Area.....	30
Chapter V: Conclusion and future trends .....	35
References .....	37
Appendices.....	43
1. Solid State Lighting.....	43
2. Color quality of white light sources .....	43
<b>2.1. Figures of merit</b> .....	43
<b>2.2. Light Sources</b> .....	46
3. Radiative and Non-Radiative Transitions .....	47
4. I1 and I2 Optoelectrical Characterization .....	48
5. Impedance spectroscopy of OLED.....	48
<b>5.1. Equivalent circuits</b> .....	49
<b>5.2. Capacitance-Voltage Measurements</b> .....	51
6. Increasing the emission area .....	52

## List of Figures

- Figure 1** – Schematic of a multi-layer Organic Light Emitting Diode (OLED) and device operation. Holes are injected through the anode while electrons are injected through the cathode. Each layer was left unnamed intentionally (adapted from [8]) ..... 5
- Figure 2** – a) Bonding in a carbon-based molecule with  $sp^2$  hybridization. b) Benzene molecule and its delocalized states forming the LUMO and HOMO levels (adapted from [11]). ..... 6
- Figure 3** – Hopping process in an organic molecule as a result of the orbitals overlapping (dashed lines) allowing the carrier to hop between them when an electric field is applied..... 7
- Figure 4** – IV dependence with the applied voltage in an organic semiconductor considering a trap-free and a trap-dependent (either shallow or deep) model. The effects of the trapped carrier in the mobility is not described. The dynamics of the junction created between a metal and an organic semiconductor can be found in [17]. ..... 8
- Figure 5** - State of the art on applied structures used for white light emission on bottom emitting W-OLEDs. a) vertically stacked b) pixelated monochrome, c) single-emitter-based, d) blue OLEDs with downconversion layers, e) single OLEDs with a sublayer EML design and f) single emitting layer OLEDs based on a selective doping process. .... 9
- Figure 6** – Final device structure composed with three organic layers sandwiched between two electrodes. Adding more would allow for a more efficient device at the expense of its simplicity. The HTL is used also as EML being based on the Host:Guest system. Holes are injected into the HTL while electrons in the ETL. Finally, because electrons have lower mobility, a HBL is introduced to assure the recombination in the HTL (Chapter I section 2.1.). ..... 13
- Figure 7** – Chemical structure of all organic small molecules used for the OLED deposition. The final device structure is ITO/NPB:x%DCM1:y%C-153/BCP/Alq<sub>3</sub>/Al as anode/HTL (and EML)/HBL/ETL/cathode respectively. x% and y% stands for small %wt of the dopants. All chemical structures were purchased from Sigma Aldrich. .... 14
- Figure 8** – Schematics showing all process to obtain a small area bottom-emitting OLED from a glass substrate containing a thin ITO film (a) leading to its patterning (b), cleaning process (c) and thermal evaporation of the blend EML (d), the HBL (e), the ETL (f) and the cathode (g) respectively. 4 different emissive areas of 25 mm<sup>2</sup> (h) were produced. .... 15
- Figure 9** – Normalized Electroluminescence spectra of devices I1, I2 and I3 at 32 V. The color tuning, is achieved by the increase of the peak intensity at around 550 nm changing the overall emitted color. The significantly high voltage is the result of a high resistivity ITO film. .... 18
- Figure 10** – CIE 1931 (x, y) Chromaticity diagram for devices I1, I2 and I3 at 32 V according to the results shown in table 4. All devices clearly emit in the white region. Though device I3 emits at the greenish-white, ideally it should be closer to the reddish-white for a good warm white emitter. To improve this, another red dye can be introduced which enhances the emission at this wavelength and redshifts the overall EL. This study was not conducted in this project. .... 19

**Figure 11** - a), b), c) EL spectra for the tunable W-OLED i.e. for the devices composed with different concentration of DCM1 I1, I2 and I3 respectively. The inset on each graph shows a picture of the different device at 32 V for a naked eye interpretation. The applied voltages were 26, 28, 30 and 32 V for all samples..... 20

**Figure 12** – Normalized PL spectra of NPB, C153 and DCM1 independently. .... 21

**Figure 13** – EL spectra for a device with an active layer of NPB:1%C153 showing a slight blue-shift of C153's main emission. .... 22

**Figure 14** – Energy levels of all layers constituent of the devices (table 1). .... 22

**Figure 15** – Active layer operation. When electrons are injected, they channel to DCM1 in a non-radiative way without C153 (a) or when C153 is added (b) resulting in the emission of light through DCM1. When its concentration is decreased, the emission of C153 (c) is promoted resulted in the increase of the correspondent peak. .... 23

**Figure 16** – JVL curves for devices I1, I2 and I3. The Luminance was taken without background light to reduce ambient effects. .... 24

**Figure 17** – a) log(IV) curves for the device I3 displaying the ohmic and SCLC regions. The curve's slope is an evidence of a deep trap behavior ( $m > 2$ ). b) Efficiency dependence with voltage of device I3 for an OLED with emission area of 25 mm<sup>2</sup>. .... 25

**Figure 18** - a) Capacitance and dielectric loss curves for the device at 0 V dc typical for the ohmic regime. b) Cole-Cole plot, i.e. the dielectric loss as a function of the capacitance for the same device. Following a model described in the inset with a parallel RC for R1=110 Ω and C1=8.75 nF, a simulated curve was drawn showing a good fitting can be obtained for this model. .... 26

**Figure 19** – a) Capacitance and dielectric loss curves for the device at 20 V dc to assure the SCLC showing interfacial changes in the capacitance dielectric loss values b) Cole-Cole plot, i.e. the dielectric loss as a function of the capacitance for the same device. Following a model described in the inset with a two sets of parallel RC in series for R1=17500 Ω, R2=105 Ω, C1=9 nF and C2=0.02 nF a simulated curve was drawn showing a good fitting can be obtained for this model. The equipment interference at low frequency results in a deviation of the obtained values..... 27

**Figure 20** – Capacitance-voltage measurements of the device shown in figures 9 and 10 at a fixed frequency of 1000 Hz. .... 28

**Figure 21** – a) Capacitance and dielectric loss for the same device at 0 V dc after 0, 24, 48 and 72h at room temperature and ambient air. b) Correspondent Cole-Cole plots overlapped with its simulated curves using the R1 and C1 values of table 6 always assuming a parallel RC model. .... 29

**Figure 22** – a) Capacitance and dielectric loss for the same device at 20 V dc after 0, 24, 48 and 72h on room temperature and ambient air. b) Correspondent Cole-Cole plots overlapped with its simulated curves using the R1, R2, C1 and C2 values of table 7 always assuming a model with a series of two parallel RC..... 30

**Figure 23** – a) barrier limit OLED with an active layer of 2.25 cm<sup>2</sup>. b) JV curve for the device in figure 23a. The use of a low resistivity ITO film decreased the threshold voltage to around 11 V. Inset shows

the EL spectra for a typical barrier limit white emission. This barrier white emission was obtained for concentrations of 98.3%:1%:1 of NPB:C153:DCM1 respectively. .... 31

**Figure 24** – a) cool white OLED with an active layer of 16cm<sup>2</sup> and highlighted defects. b) JV curve for the device in figure 24a with threshold voltage of around 11 V. Inset shows the EL spectra for a cool white emission with a low emission from DCM1 which may be the result of a low material evaporation. Increasing this should increase the amount of DCM1 in the final evaporated blend. This cool white emission was obtained for concentrations of 98.3%:1%:0.7 of NPB:C153:DCM1 respectively..... 32

**Figure 25** – a) cool white OLED with an active layer of 16cm<sup>2</sup> produced with an optimized ITO patterning. b) JVL characteristic for this device showing a voltage drop for the threshold voltage as a result of a decrease in the ITO's resistivity. .... 33

**Figure 26** – CIE 1931 (x,y) including different color regions, planckian locus and color temperatures [2]..... 44

**Figure 27** – The effects of light sources with high (90) and low (60) Color Rendering Indexes. A high CRI means that a color source effectively covers the entire visible spectrum being able to reproduce all the surrounding colors. Low CRI, on the other hand, may lack Red, Green or Blue counterparts resulting in inefficient reproducibility of the surrounding environment. (adapted from [63])..... 45

**Figure 28** – CCT values for different sources including range for the produced OLEDs. .... 45

**Figure 29** – Energy transitions in a Host:Guest system (section 2.1.) namely the energy transfer (either through radiative a) and non-radiative i.e. the Förster transition b)) and the carrier trapping c). .... 47

**Figure 30** – a) JV curves and b) current efficiency values for devices I1 and I2..... 48

**Figure 31** – IV curve of an ideal diode. For IS measurements, a bias voltage  $V_{DC}$  is chosen followed by the appliance of an alternating signal  $V_{AC}(t)$  and the corresponding  $I_{AC}(t)$  is obtained. [60] ..... 48

**Figure 32** – Models considered for an IS analysis based on a) single and b) double parallel RC circuits ..... 50

**Figure 33** – CV measurement of an OLED device. The values were left out purposely being of particular interest the behavior and not the constitution of the device (adapted from [60]) ..... 51

**Figure 34** – geometric capacitance of the device analyzed for a)  $V < V_t$  and b)  $V_t \leq V < V_{bi}$  based on eq. 5.26,  $C_2 > C_1$ . .... 52





## List of Tables

<b>Table 1</b> – Parameters considered upon the deposition of each material. Because the dyes' concentration was small compared to the Host's, its density values were not taken into consideration. ....	14
<b>Table 2</b> – blend combinations studied for the production of the color tunable white OLEDs. ....	17
<b>Table 3</b> – Blend concentration for each sample produced. In order to decrease the number of degrees of freedom, one of the concentrations was kept constant, in this case the Coumarin-153. The experiments conducted that showed that the white color in our devices is more susceptible to changes with DCM1. ....	17
<b>Table 4</b> – Figures of merit for devices I1, I2 and I3 at 32 V calculated from the relative intensity of all three devices (figure 9). ....	18
<b>Table 5</b> – Color coordinates for devices I1, I2 and I3 at voltages between 26 and 32 V corresponding to the EL spectra shown in figure 3. ....	20
<b>Table 6</b> – Simulated C1 and R1 with calculated relaxation frequency for the device characterized on figure 21 after 0, 24, 48 and 72h. ....	30
<b>Table 7</b> – Simulated C1, R1, C2 and R2 with calculated relaxation frequency, $f_{r1}$ and $f_{r2}$ , for the device characterized on figure 19 after 0, 24, 48 and 72h. ....	30
<b>Table 8</b> – Basic EL spectra of different light sources and corresponding CCT and CRI values for comparison purposes with the result obtained with this project.[59].....	46



## **Objective**

---

Organic Light Emitting Diodes (OLEDs) promise to shape the entire reality of general lighting technologies. This thesis aims to produce Color tunable White OLEDs (W-OLEDs) based on a single doped RGB active layer. The color tunes are obtained by changing one of the dopant's concentration, being the different tunes analyzed. Once the proper tunes are obtained, the scale up of the devices to large area was attempted.

## **Work structure**

---

For a better analysis, this written document is organized as follows: The motivation gives some insights on the overall applications for the project itself, both in terms of artificial lighting and simulating the entire daylight behavior as a means to stimulate productivity and promote health. Then, chapter I describes some basic knowledge regarding the OLED operation followed by the formation of the energy diagrams (1.1.), charge transport (1.2.) and how light is emitted (1.3.). Given this, the structures applied for the W-OLEDs are reviewed on section 2, including the main mechanisms happening in a Host:Guest system. Chapter II reviews the basic structure, materials and considerations used for this project and Chapter III describes all the experimental details for the device production and characterization. The devices produced are characterized in section IV divided in terms of blend definition (1), the physics behind the operation (2), the optoelectrical characterization (3), the a.c. analysis (4) and the application on Large Area substrates (5). Chapter V summarizes the main conclusions sharing also some threads on where to perceive next. This document also includes a set of appendixes to explain some notions needed during the entire document such as the review in terms of Solid State Lighting (1), The Color quality of W-OLEDs (2), the radiative and non-radiative transitions diagram (3), other optoelectrical characterization not focused on Chapter IV (4), the Impedance Spectroscopy (IS) studies (5) and what happens when the emission area is increased (6).



## Motivation

---

### 1. Towards OLED lighting

The energy demand nowadays has brought an exhausting use of the natural resources. Considering that 19% of all the electricity consumed is for artificial lighting which corresponds to an emission of 1900 Mt of CO<sub>2</sub> every year [1], improvements towards a more eco-friendly future is urgent.

Looking for the “ideal” lighting system, the research for a power efficient, disposable, non-harmful and long-lasting technology is thought. And throughout history, many attempts have been made to effectively reach this ideal technology, each of them lacking one or more of the goals referred as it will be explained further ahead.

The scientific community has been looking for more efficient ways to produce light. Appendix 1 shows how this technology has been evolving resulting in the commercially available Light Emitting Diodes (LEDs) which are more economical and have longer lifetimes than the past bulb and fluorescent lamps. However, LEDs have several limitations since most of them use rare materials such as Ga, As, In, etc. and soon enough problems of scarcity can be faced. [2]

Organic Light Emitting Diodes (OLEDs) come to help solving this problem since they use organic materials instead of inorganic and can be produced in a large set of substrates (which includes large area panels). [3] Therefore, it can shake the current lighting paradigm as a not so futuristic technology (not anymore at least) since it allows for a materials’ internal efficiency of, theoretically 100%, can be fabricated in rigid or flexible substrates, uses organic disposable materials with zero harm to the environment and allow for the possibility of obtaining high brightness devices. All of this not mentioning its market attractiveness. Putting together all these qualities, OLEDs have a huge market interest in the near future for the everyday life’s artificial lighting. The market of OLEDs is already ON and soon can replace the current LED technology.

### 2. The circadian rhythm

It is interesting to analyze the color tuning ability that OLED devices may achieve. Theoretically, by simply changing the materials (or their proportion) or the overall device structure, it is possible to obtain sources capable of emitting different shades of white specific environments and applications. But, forgetting the obvious academic and artistic interest what is the main market interest here? Why should we care if we are surrounded by a cool white (with blueish tone) or a warm white source (with a greenish/reddish tone)?

Life on Earth is controlled by the 24h hours of the solar cycle that synchronizes the biological circadian cycle (or rhythm) with physiology and behavior patterns with light serving as a reset of this rhythm. And we are surrounded by light, either environmental or artificial. This last one aims to reproduce the surrounding colors in the absence of environmental light. The problem is that these sources don’t follow the same light pattern of the solar cycle, having a direct effect in the biologic one.

After studies in animals had suggested a role for a non-rod, non-cone photoreceptor in circadian responses to light, melanopsin was identified as the photopigment present in those specialized photoreceptors. In this matter, critical to our sleep/wake cycle is melatonin, segregated by the hypothalamus, a hormone that promotes sleep, and can be stimulated by the kind of light we are surrounded to due to special non-visual photoreceptors at the retina stimulated with the blue color. It is also being used as a sleep aid and in the treatment of some sleep disorders. [4] So depending on the surrounding light, this hormone can be segregated or inhibited. Morning light, for example, is light that is received during the first hours of the day and is very effective at resetting the rhythm. Getting strong blue rich light early in the morning every day helps to stay in tune with the timing of daily obligations since bluish white light stops melatonin production. Evening light, on the other hand, as long as it is dim and low in blue (short wavelength) content, can help relaxing and prepare for sleep (yellowish white light allows for melatonin production). [5] Bright evening light, though, suppresses melatonin production and delays sleep. And this is where the target application comes in place.

By producing sources capable of emitting different tones of white, it is possible to adapt the ambient artificial light to 1) behave similarly to the environmental one and regularize the circadian rhythm with the solar cycle or 2) promote productivity with the control of melatonin production. So, because OLEDs may offer efficient ways of emitting wavelengths with different temperatures that could range the entire daylight behavior, they could be adapted to artificial light, as they are passive for a low cost device production with high stability.

## Chapter I: Introduction

### 1. Organic Light Emitting Diode's operation

Tang and VanSlyke (1987) and Burroughes et. al. (1990) were the first to report low voltage electroluminescence from thin organic films made of small-molecular-weight molecules and polymers, respectively. Ever since, the possibility of applying organic materials on lighting systems has emerged and research on this topic has brought a big increase on the number of reports regarding this subject. The possibility of light emission from organic materials has, therefore emerged a wider range of possibilities, being the first step towards the recent developments of Organic LEDs (OLEDs) and Polymer LEDs (PLEDs).[6],[7]

An OLED is a lighting device capable of emitting white light through the use of organic molecules. Generally, these devices are composed of different organic layers sandwiched between two electrodes. A diagram describing the main operation of OLEDs can be found in figure 1. Each layer has a different purpose in the overall working of the device, so each organic material (either small molecule or polymer) must be chosen according to their function in the final structure. The main mechanism, is similar to the Light Emitting Diode's (LED) behavior. [8]

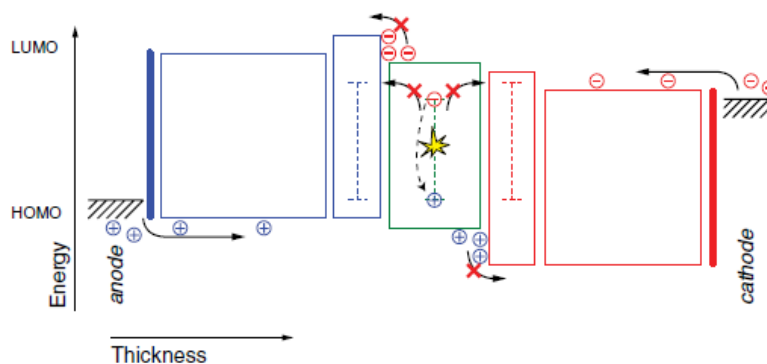


**Figure 1** – Schematic of a multi-layer Organic Light Emitting Diode (OLED) and device operation. Holes are injected through the anode while electrons are injected through the cathode. Each layer was left unnamed intentionally (adapted from [8])

Upon application of an external bias, electrons and holes are injected by the electrodes into the p and n organic layers, travelling across their molecular structure until they recombine in the emissive area. Here, excitons (coupled state between electrons and holes) are formed through Coulomb interaction between the injected carriers in a process called charge recombination. The rapid decay of the electron to a lower energy state, allows for the emission of light with a wavelength corresponding to the energy transition of the carrier where the emission takes place. [9], [10]

#### 1.1. Hybridization in Organic Semiconductors

The carrier behavior in an organic semiconductor is a result of the nature of the carbon bonds and the molecular orbital structure of the organic semiconductors. Each carbon atom has two incomplete 2p orbitals (its configuration is  $1s^2 2s^2 2p^2$ ), allowing the formation of hybridized orbitals  $sp$ ,  $sp^2$  or  $sp^3$  between other atoms in order to form the lowest energy bonds possible. In this case,

the nature of the  $sp^2$  bonds gives rise to carrier conduction forming, for example, the benzene ring that will serve as an example further ahead. In this type of hybridization (figure 2a), there are three hybrid  $sp^2$  orbitals and one  $2p_z$  that allows for the formation of three high energy  $\sigma$  bonds (one per each hybrid orbital) and two low energy  $\pi$  (one bonding, denoted  $\pi$  and one antibonding, denoted  $\pi^*$ ). When the benzene ring is considered (figure 2b), with a configuration  $-C=C-C=C-C=C-$ , the double bonds are composed by one  $\sigma$  and one  $\pi$  and because this last one is of low energy, the electrons can, under an electrical field, move throughout the molecule in delocalized states (not associated with an atom but within an orbital of several adjacent atoms).

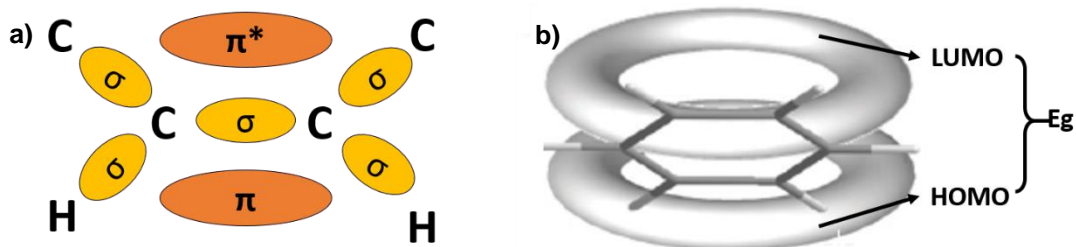


**Figure 2** – a) Bonding in a carbon-based molecule with  $sp^2$  hybridization. b) Benzene molecule and its delocalized states forming the LUMO and HOMO levels (adapted from [11]).

Increasing the number of carbon atoms in the molecule, an energy cloud composed with these delocalized electrons and their ability to roam freely in the molecular orbital is formed. These occupied states, more specifically the highest energy counterpart, forms the so called Highest Occupied Molecular Orbital (HOMO). The antibonding unoccupied states  $\pi^*$ , or its lowest energy counterpart forms the Lowest Unoccupied Molecular Orbital (LUMO). Between the HOMO and the LUMO of each material is the so called energy gap,  $E_g$  prohibited for the delocalized electrons.[11],[12]

These energy levels are a characteristic of the organic semiconductor the same way the valence and the conduction band are a characteristic of an inorganic one. By using different layers composed of different materials, a structure capable of guiding carriers through the organic layers is built by either enhancing their injection or promoting their blockage always having in mind the differences in charge mobility (chapter I section 1.2.1.). It is then possible to denote different layers according to 1) the charge it relates to (hole or electron) and 2) its basic function (injection, transport or blockage) giving rise to the Hole and Electron Injection (HIL and EIL respectively), Transport (HTL and ETL respectively) and Blocking (HBL and EBL respectively) layers. Finally, the layer where recombination and emission takes place is called Electroluminescence Layer (EML).

## 1.2. Charge Transport

### 1.2.1. The Hopping process

Once available for conduction, electrons and holes travel freely across the inorganic semiconductor's matrix in the conduction and valence bands, respectively. Carrier transport in organic semiconductor based devices, on the other hand, is different from this behavior. It is based on a hopping process (figure 3) - interference between the delocalized orbitals  $\pi$  and  $\pi^*$  with the applied electric field. As seen before, the main consideration is the typical structure of the benzene ring where



the electron cloud results from the overlapping of the orbitals. An electron in one of these LUMO orbitals, although still connected to its original carbon atom, is susceptible to hop into a neighbor orbital if an electric field is applied, vacating it and allowing for another electron to hop into it. This carrier transport gives rise to the electrical conduction. A similar behavior can be seen in the HOMO orbitals for the hole conduction. This process will have a big effect on the carrier mobility. Although delocalized, the carrier never loses the identity to its atom counterpart, so the mobility will be several orders of magnitude lower than a carrier travelling in an inorganic semiconductor. Also, the bonding delocalized orbital has a more consistent structure than the non-bonding resulting in a higher mobility for HOMO's holes in the when compared to the LUMO'S electrons.[13]

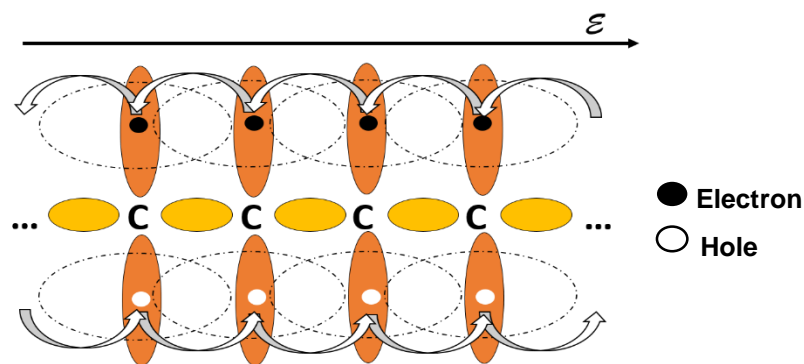


**Figure 3**– Hopping process in an organic molecule as a result of the orbitals overlapping (dashed lines) allowing the carrier to hop between them when an electric field is applied.

### 1.2.2. Space Charge Limited Current

When carriers are injected into their layers, i.e. when a voltage is applied, the unorganized structure of the organic semiconductors compared to the organized for the inorganic, implies a completely different behavior for carrier conduction. The models describing the timeframe after the carriers are injected into the organic layers are shown in figure 4.

At low applied voltages, even using electrodes with considerably different energy barrier in the metal semiconductor junction, both anode and cathode are able to equally inject the same amount of carriers being the current only dependent on the resistance of the material – **Ohmic region** where  $I \propto V$ . Increasing the applied voltage until a certain value (Ohmic regime limit voltage,  $V_{\Omega}$ ) leads to a difference in the injection performance of the electrodes if, in a finite time, one of them is considerably different from the other, meaning that one electrode is effectively injecting a carrier while the other is ineffectively pushing it which leads to an increase of current inside the device – **Space Charge Limited Current (SCLC) region** where  $I \propto V^n$  and  $n > 1$ .

In the SCLC, the unorganized structure allows the appearance of traps that may fall within the energy gap of the semiconductor. To analyze the effects of these traps, considering first a trap-free model and comparing it with two trap-dependent models, each one categorized by their proximity to the Fermi level: shallow trap if it is energetically close or deep trap if far. In the **trap-free model**,  $n=2$  as a result of no trapping of carriers, meaning that the current flows accordingly to the mobility of these carriers and the physical and electrical properties of the layer. In the **shallow-trap model**, the

trapped carriers do not contribute to the current, leading to its decrease, but still dependent on  $V^2$ . Increasing the applied voltage, all traps will eventually be filled. Near this limit voltage value (Trap Fill Limited Voltage  $V_{TFL}$ ), there's a slight increase in the current ( $V^n$  with  $n > 2$ ) followed by the same behavior described before. Finally, for the **deep-trap model**, a discrete distribution of traps is considered and different models must be applied to better describe the transport mechanisms. By considering either a Gaussian or an Exponential distribution, the behavior is similar only characterized by different expressions, for  $V_{\Omega} < V < V_{TFL}$ , the current is dependent of  $I \propto V^n$  and  $n > 2$ . Above  $V_{TFL}$  the exhibited behavior is the same as described before.[14], [15], [16]

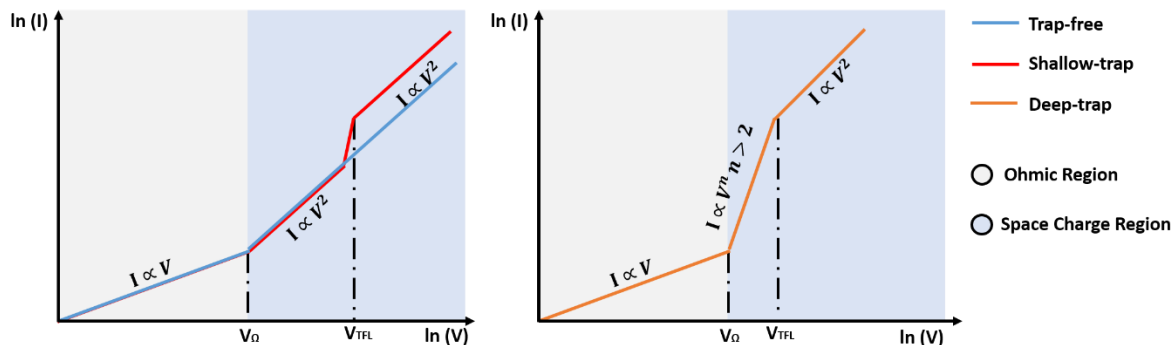


**Figure 4** – IV dependence with the applied voltage in an organic semiconductor considering a trap-free and a trap-dependent (either shallow or deep) model. The effects of the trapped carrier in the mobility is not described. The dynamics of the junction created between a metal and an organic semiconductor can be found in [17].

### 1.3. Light Generation: Fluorescence and Phosphorescence

Light is emitted whenever there's radiative decay (emission of a photon) of an electron from an excited energy level to the fundamental state, being the wavelength of the photon emitted equivalent to the energy decay of that electron. In organic semiconductors, this radiative decay is a result of the recombination between carriers to form an exciton.

Understanding the difference between fluorescence and phosphorescence implies knowledge of electron spin and the differences between singlet and triplet states. When an excitation occurs from the fundamental state and depending on the spin of the level it achieves, there are two types of excited levels. In terms of terminology, a singlet (triplet) state occurs when the spin of an electron in the  $\pi^*$  orbital and that of the remaining electron in the  $\pi$ -orbital are antiparallel (parallel) and so add up to a total spin of zero (one). Therefore, because a singlet exciton has a spin multiplicity of 0 ( $M_s = 0$ ) and the triplet exciton 1 ( $M_s = -1, 0$  and 1), on average 75% of the excitons formed are triplet states, with the remaining 25% being singlets. In the fundamental state, electrons have non-paired spins, typical of a singlet level. The triplet state has a smaller energy than its singlet counterpart because of the repulsive origin of its electron spins.

In OLEDs, both radiative and non-radiative transitions may occur. If this transition happens between singlet levels ( $S_1 \rightarrow S_0$ ) it is called fluorescence which is the most common between small molecules because of small permanence time (large transition probability) in the excited singlet. This limits the theoretical device efficiency to the probability of singlet-to-singlet transition, 25%. If the

transition involves a triplet-to-singlet state ( $T_1 \rightarrow S_0$ ) it is called phosphorescence, though this implies the use of intermediate materials (such as rare earth or transition metals) for radiative transition that reduce the permanence time (increasing the transition probability) of an electron in the excited triplet state. Otherwise, the energy loss would be made by thermally (i.e. non-radiatively). Phosphorescent devices have a theoretical efficiency up to 100% as it considers both singlet-to-singlet and triplet-to-singlet transitions.[3],[18],[19] This results in devices with considerably higher external efficiency. [20]

Recently, there have been reports on Thermally Activated Delayed Fluorescence (TADF) to achieve 100% efficiency on fluorescent materials via Reverse Intersystem Crossing (RISC) which is based on the use of temperature to allow for the transition of an electron from an excited triplet to an excited singlet. [21]

## 2. W-OLEDs for Solid State Lighting

When lighting is concerned, the main focus is to have emission from the entire visible spectrum – white light. When OLEDs are concerned, many structures have been attempted to effectively achieve this (figure 5). The first White OLED (W-OLED) dates back to 1995 created by Kido. [22]

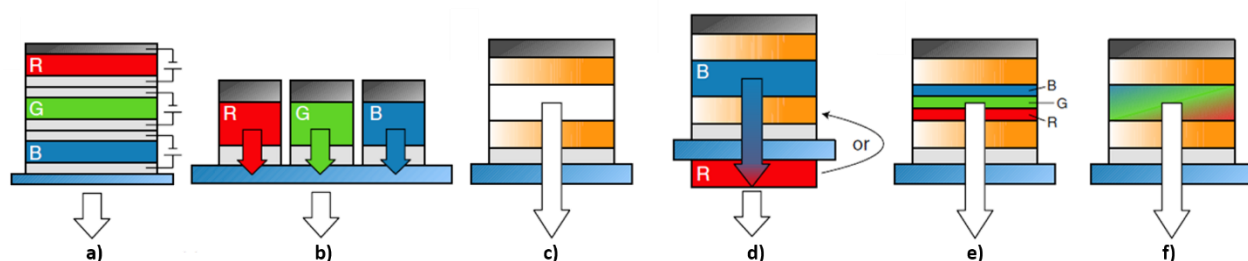


**Figure 5** - State of the art on applied structures used for white light emission on bottom emitting W-OLEDs. a) vertically stacked b) pixelated monochrome, c) single-emitter-based, d) blue OLEDs with downconversion layers, e) single OLEDs with a sublayer EML design and f) single emitting layer OLEDs based on a selective doping process.

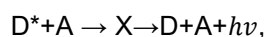
Figure 5 a) and b) shows the emission of white light as a sum of independent Red, Green and Blue emitters either with individual electrodes or as a pixelated structure, commonly used on the current OLEDs flat panel displays. These two structures involve comparably complicated structuring processes which would increase the final production costs'. [23], [24] So, in order to decrease these, a single emitting layer must be considered. A single molecule, for example, may be synthesized to emit over the entire visible spectrum (figure 5c) although it is not easy to tune the color without affecting device performance. Also, these molecules are usually related to poor device efficiencies [20] [25] The use of an external (or internal) downconversion layer (figure 5d) is based on high energy emissions. Part of this light excites another molecule resulting in its main emission, the sum being white light. This implies a slightly more complicated structure (one or two downconversion layers) than the single emitting layer, while resulting also in poor color rendering because of poor overlapping between the high energy layer's excitation and the downconversion layer's absorption. [26], [27] To overcome this problem, a single layer capable of emitting RGB wavelengths from sublayers (figure 5e) or based on a selective doping process - the Host:Guest system (figure 5f) - have also been attempted, this last one described more extensively in this thesis. The main conclusion taken from

here is that there must be a trade-off between the device complexity and efficiency when lighting is concerned. So far, there has not been a report of a blended RGB capable of efficiently emitting with a great level of stability. [28] To assure the highest quality for the lowest complexity, either the emissive layer or the whole device must be tailored. The purity of a white source can be characterized by the corresponding figures of merit, described more extensively on appendix 2: the Commission Internationale de L'éclairage (CIE), the Correlated Color Temperature (CCT) and the Color-Rendering Index (CRI). Also, devices with high color stability with the applied voltage/current prevent shifts in terms of CIE that will be perceived by the human eye. [29]

### 2.1. Selective doping – the Host:Guest System

The Host:Guest System is the most used technique to obtain white light since it allows for the production of simple devices with high efficiency. [30] This system consists of a single EML comprising one host matrix – donor – and one or more dopants – acceptor dyes – mixed inside the matrix allowing for light emission in these materials. It involves two predominant mechanisms: the energy transfer and the carrier trapping. Considering the energies' corresponding vibrational levels of the fundamental state  $S_0$  and excited state  $S_1$  of both donor and acceptor molecules, one can easily draw the schematics of these main mechanisms (appendix 3).

The **energy transfer**, more specifically, can be a result of radiative and non-radiative transitions. In the radiative transition, after an excitation of a donor electron to its excited level and subsequent energy loss by non-radiative transitions – phonons – to the lowest excited level, a photon with lower energy is emitted. This photon will then be absorbed by the acceptor resulting in the transition of one of its electrons from the fundamental state to the excited level of the guest. After energy relaxation, photons with wavelengths of the corresponding final radiative transitions are emitted (appendix 3, figure 29a). This process will only happen if there is an overlap between the emission of the dopant and the absorption of the acceptor. The non-radiative transition involves a dipole-dipole interaction with long-range separation ( $\sim 30\text{-}100 \text{ \AA}$ ) between an excited electron of the donor and an electron in the fundamental state of the acceptor (and their corresponding holes) allowing it to transfer energy electrostatically, also known as **the Förster transition** (appendix 3, figure 29b).[31] [32] This energy transfer can be explained as



where  $D^*$ ,  $A$ ,  $X$ ,  $D$  and  $h\nu$  stand for excited donor, ground state acceptor, intermediate excited state (ground state donor and excited acceptor), ground state donor and acceptor and energy of the emitted photon, respectively. [33] A short range interaction known as the Dexter transition, is not considered because the host and guest molecules will fall far from the Dexter range. [31]

In the **carrier trapping**, the guest's HOMO and/or LUMO levels must fall within those of the hosts' to allow for an easy non-radiative trapping of the charge carriers under low voltage, resulting in the emission of light through the guest (appendix 3, figure 29c). Increasing the applied voltage promotes an increase of the carriers in the energy levels of the dopants gradually filling all their traps. Once this is obtained, the recombination in the dopants stops and saturation is achieved. [34]

All mechanisms may be equally present resulting in big color shifts with the applied voltage, which affects the color stability of the device. To prevent this, the dopant concentration is kept low while assuring that the average spacing between the dye molecules is less than the Förster distance leading to the saturation of traps and prevention of the non-radiative interaction between molecules, respectively. In order to understand which mechanism is taking place, one has to compare the Electroluminescence (EL) and Photoluminescence (PL) spectra of the device and corresponding materials. Other reports include the same system but employ a mixed-host structure to promote host-guest stability. [35]



## Chapter II: Materials and Structure

The device's physical characteristics must be tailored to optimize the structure and stabilize white light emission while also meeting the requirements of a Solid State Device – simple and efficient. This project's device (figure 6) has three organic layers between the electrodes. The final device structure is: Anode/HTL/HBL/ETL/Cathode with the HTL serving also as EML based on the Host:Guest system (Chapter I, section 2.1.). Finally, because all of the organic materials used are small molecules, a thermal evaporation technique is used.[36] Figure 7 shows the chemical structure of the final organic molecules used to build each device while table 1 describes the basic parameters important for device production and characterization.

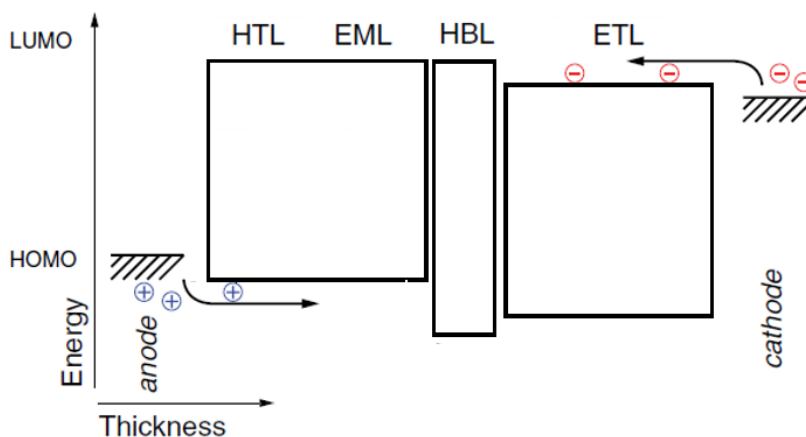
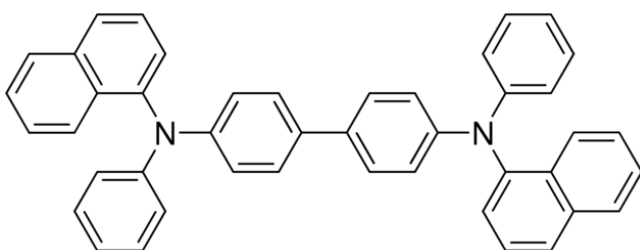
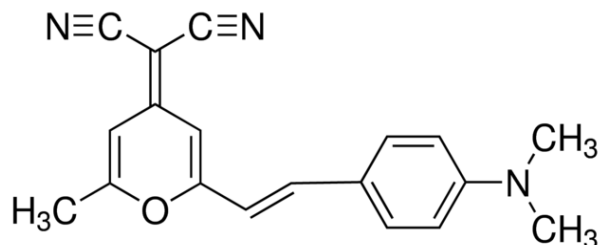


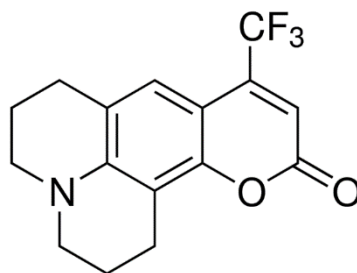
**Figure 6** – Final device structure composed with three organic layers sandwiched between two electrodes. Adding more would allow for a more efficient device at the expense of its simplicity. The HTL is used also as EML being based on the Host:Guest system. Holes are injected into the HTL while electrons in the ETL. Finally, because electrons have lower mobility, a HBL is introduced to assure the recombination in the HTL (Chapter I section 2.1.).



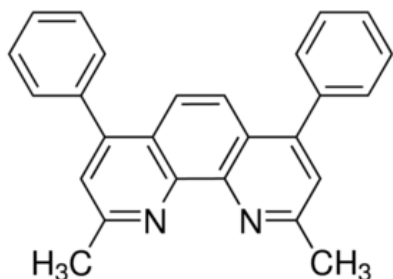
**NPB (Blue Host)**



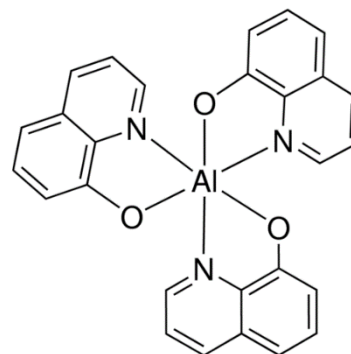
**DCM1 (Red Guest)**



**Coumarin-153 (Green Guest)**



**BCP (HBL)**



**Alq<sub>3</sub> (ETL)**

**Figure 7** – Chemical structure of all organic small molecules used for the OLED deposition. The final device structure is ITO/NPB:*x*%DCM1:*y*%C-153/BCP/Alq<sub>3</sub>/Al as anode/HTL (and EML)/HBL/ETL/cathode respectively. *x*% and *y*% stands for small %wt of the dopants. All chemical structures were purchased from Sigma Aldrich.

**Table 1** – Parameters considered upon the deposition of each material. Because the dyes' concentration was small compared to the Host's, its density values were not taken into consideration.

	Organic Material	Function	HOMO (eV)	LUMO (eV)	Density (g/cm <sup>3</sup> )	Melting Point	Ref.
Small Molecules	NPB	Host/EML/HTL Blue Emitter	5.5	2.4	1.664	279-283 °C	[37],[38]
	BCP	HBL	6.7	3.2	1.173	279-283 °C	[39],[40]
	Alq <sub>3</sub>	ETL	6.0	2.7	1.443	>300 °C	[39],[41]
Dyes	DCM1	Red-Orange emitter	5.6	3.5	NR	215-220 °C	[42],[43]
	Coumarin-153	Green emitter	5.3	2.9	NR	164-168 °C	[44]



## Chapter III: Experimental

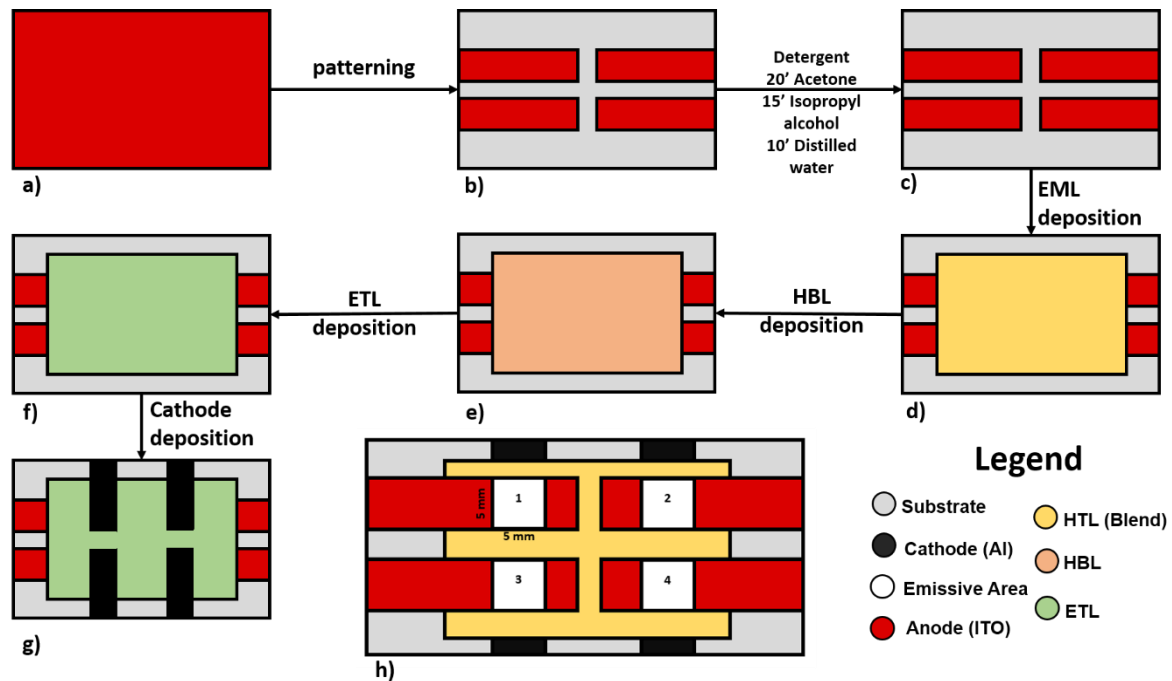


**Figure 8** – Schematics showing all process to obtain a small area bottom-emitting OLED from a glass substrate containing a thin ITO film (a) leading to its patterning (b), cleaning process (c) and thermal evaporation of the blend EML (d), the HBL (e), the ETL (f) and the cathode (g) respectively. 4 different emissive areas of 25 mm<sup>2</sup> (h) were produced.

The production (figure 8) and characterization of OLEDs follows a strict procedure which includes three main phases.

### 1. Substrate and Sample Preparation

In glass substrates with a thin ITO film deposited (a) (30-60  $\Omega$ /sq from Delta Technologies), adhesive tape was used to cover the desired patterns for the electrodes (either small or large area). With a mixture of Zinc Powder and Hydrochloric Acid, the uncovered ITO was removed, (b) followed by washing in water and removal of the tape. The substrates were then cleaned in detergent, then washed in Acetone for 20 min, Isopropyl alcohol for 15 min and distilled water for 10 min (c). The samples used as EML were weighed and then mixed under magnetic stirring for no less than 2 hours.

### 2. Films Deposition

Most of the work was conducted in the Physics department at the University of Aveiro and the large area devices were produced in CeNTI – Centre for Nanotechnology and Smart Materials.

Each substrate was loaded into the thermal evaporator chamber. The evaporation was conducted using two different high vacuum thermal evaporation chambers with control over the thickness of the films of 1  $\text{\AA}$  and deposition rate of 0.1  $\text{\AA}$ /s. For the small scale devices, a Criolab with a manual control was used with 4 crucibles (1 per each layer deposited) which is put under high vacuum through a

turbomolecular pump was used. The large scale devices were produced using a Kurt J. Lesker Spectros 150 automated system, containing 5 crucibles and a cryogenic pump for high vacuum to a closer-to-industry production.

With a pressure of no higher than  $10^{-5}$  Pa the evaporation process starts. To control each layer's final thickness, a high sensitivity piezoelectric sensor is used and, by changing the applied power, the evaporation rate is controlled to a maximum value of 4 Å/s to allow for uniform films. All blend (d) tests (50 Å thick) were followed by the deposition of 100 and 300 Å of BCP (e) and Alq3 (f) respectively. Finally, aluminum (g) was deposited with a thickness of 1500+/-200 Å. To prevent aluminum oxidation and/or diffusion into the organic layers, the chamber was stored in vacuum for 15 minutes to cool down after deposition.

### **3. Device Characterization**

All the current density–voltage (JV), luminance–voltage (LV), electro-luminescence (EL), Impedance Spectroscopy (IS) and Capacitance-Voltage (CV) measurements were performed in air in non-encapsulated devices at room temperature right after each evaporation process. For the EL spectra measurement, an Ocean Optics USB4000 spectrometer was used. The JVL characteristics were measured with a Keithley source meter 2425 model and Minolta Colormeter LS-100. From the JVL data, the current efficiency (cd/A) was calculated, a typical parameter in the light emitting devices. In parallel, the dynamic range of the light emission (the applied voltage region where the emission is quite linear) was obtained from the photometric efficiency obtained with the LV graph. IS and CV measurements were performed with a Fluke PM6303 RLC Meter. The photophysical properties – Photoluminescence (PL) and Photoluminescence Excitation (PLE) – were obtained in a Fluorolog-3 Horiba Scientific modular equipment with a double additive grating Gemini 180 scanning monochromator (2×180 mm, 1200 gr.mm<sup>-1</sup>) in the excitation and a triple grating iHR550 spectrometer in the emission (550 mm, 1200 gr.mm<sup>-1</sup>).

## Chapter IV: Results and Discussion

### 1. Blend Definition

As previously discussed, the main objective was to produce color tunable W-OLEDs based on a single emitting RGB blend that, by changing the concentration of one of its components, would allow for a set of devices **capable of emitting different types of white light** (from cool to warm). To obtain a **low complexity structure**, the Host:Guest system with a blue emitting host doped with a green and a red guest dyes, was considered. Also, besides the color tuning ability, the devices should be flexible in terms of the applied potential, i.e. its **color properties should remain the same** for the human eye when different voltages were applied. To effectively achieve these properties, many blends were studied, and all their Current Density-Voltage-Luminance (JVL) and Electroluminescence (EL) characteristics studied in order to effectively choose the best blend possible for the desired characteristics. Table 2 shows the main blends studied using different Coumarin-related and DCM-related green and red wavelengths, respectively always having NPB as blue emitting host. Ir(ppy)<sub>3</sub> was also considered for green dye but, because this is a phosphorescent material (see section 1.3.) and the results weren't improved, it was later replaced. The best combination (bold) have its materials shown in figure 7 and the concentrations used in table 3.

**Table 2** – blend combinations studied for the production of the color tunable white OLEDs.

HOST	DYE1	DYE2
NPB	Coumarin-500	DCM1
NPB	Coumarin-6	DCMS
NPB	Coumarin-153	-----
NPB	-----	DCMS
<b>NPB</b>	<b>Coumarin-153</b>	<b>DCM1</b>
NPB	Ir(ppy) <sub>3</sub>	DCM1

**Table 3** – Blend concentration for each sample produced. In order to decrease the number of degrees of freedom, one of the concentrations was kept constant, in this case the Coumarin-153. The experiments conducted that showed that the white color in our devices is more susceptible to changes with DCM1.

SAMPLE	HOST	DYE1 (x)	DYE2	Terminology
I1	NPB	DCM1 (0.5% wt.)	Coumarin-153 (1% wt.)	Cool White
I2	NPB	DCM1 (0.7% wt.)	Coumarin-153 (1% wt.)	Barrier Limit White
I3	NPB	DCM1 (1% wt.)	Coumarin-153 (1% wt.)	Warm White

Comparing this structure to other reports, this one is much simpler (only three organic layers) which goes accordingly to the application in mind. [45] Next sections show the main characterization for each sample considered on table 3. Each device was built at least twice to verify the reproducibility of the final structure. The best result of each test is, therefore shown though they didn't present significant differences.

## 2. Device Dynamics

### 2.1. Electroluminescence Spectra and Figures of Merit

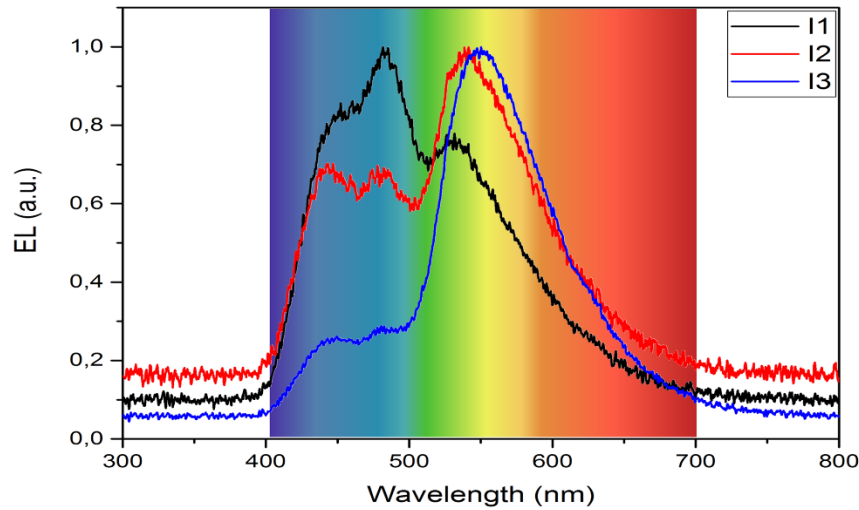


**Figure 9** – Normalized Electroluminescence spectra of devices I1, I2 and I3 at 32 V. The color tuning, is achieved by the increase of the peak intensity at around 550 nm changing the overall emitted color. The significantly high voltage is the result of a high resistivity ITO film.

Figure 9 shows the EL spectra of devices I1, I2 and I3 overlapped with the visible spectrum. The main emission covers almost the entire visible region with a lower evidence between the 625 and 700 nm. By increasing DCM1's concentration, the middle peak at around 475 nm decreases indicating an interaction between different materials. Also, the third peak slightly redshifts from around 535 to 550 nm and its relative intensity increases which indicates that this belongs to the emission of DCM1. With these interactions, the color tuning is achieved with DCM1 concentrations ranging from 0.5% (cool white) to 1% (warm white) with its barrier limit white at around 0.7%. This effect is therefore translated in terms of the correspondent figures of merit (appendix 2) shown in table 4 where the color coordinates (figure 10) change but always stay within the white region. The devices also show high values of CRI meaning a high capability of reproducing the colors of an object when illuminated with these sources, similar to other light sources (appendix 2.2.) proving the applicability of this device to general lighting. The CCT range goes even further than the typical known range for LEDs, 3000 to 7000 K (appendix 2.1.), allowing for a wider range of color tunes.

**Table 4** – Figures of merit for devices I1, I2 and I3 at 32 V calculated from the relative intensity of all three devices (figure 9).

SAMPLE	CIE <sub>x</sub>	CIE <sub>y</sub>	CRI	CCT (K)
I1	0,238	0,317	91 ± 2	10500
I2	0,296	0,389	90 ± 2	5100
I3	0,375	0,484	89 ± 2	3200

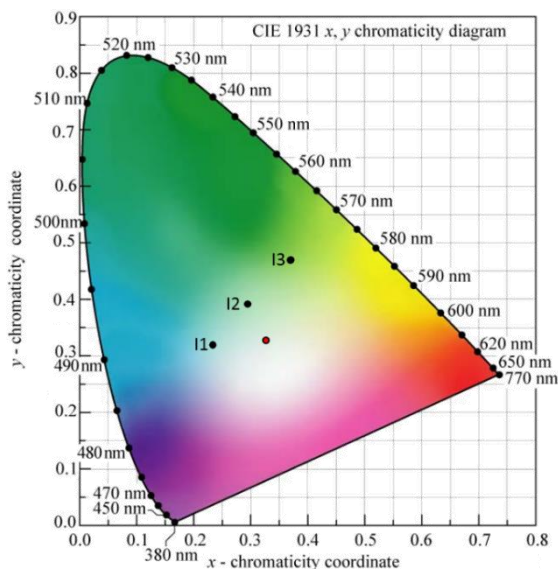
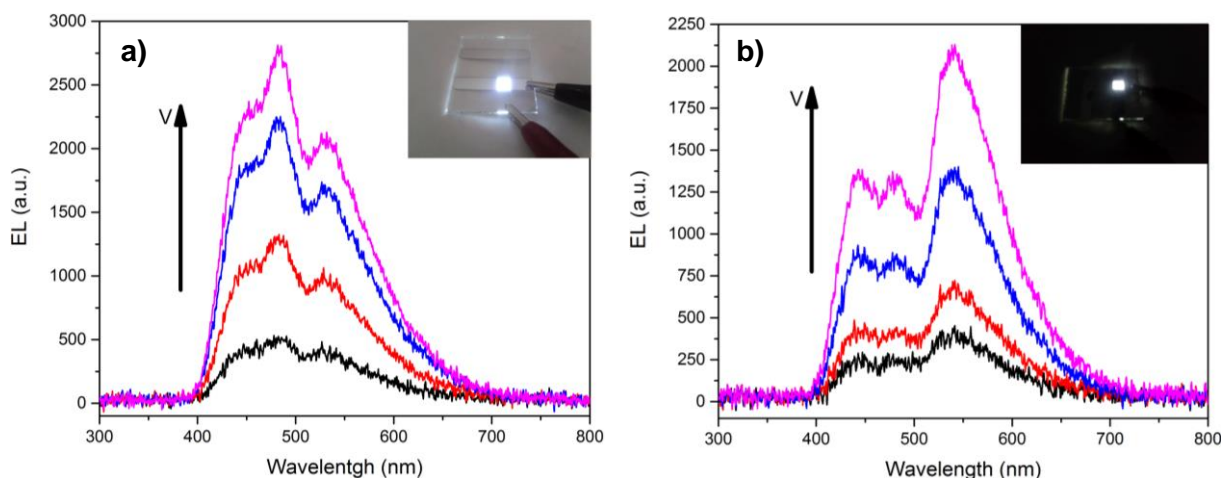


**Figure 10** – CIE 1931 (x, y) Chromaticity diagram for devices I1, I2 and I3 at 32 V according to the results shown in table 4. All devices clearly emit in the white region. Though device I3 emits at the greenish-white, ideally it should be closer to the reddish-white for a good warm white emitter. To improve this, another red dye can be introduced which enhances the emission at this wavelength and redshifts the overall EL. This study was not conducted in this project. The red point represent the Equal Energy White (EEW) coordinates (0.33, 0.33).

The evaporation process didn't offer a temperature controlled evaporation but, as the results were reproducible, it is safe to assume that the concentrations were correct. Still, this is just a supposition as a more detailed study must be conducted.

## 2.2. Device Stability

To assess on the stability of a lighting source, different voltages were applied across the device and the overall emission studied. Figure 9 already showed the main emission of the set of devices at 32 V but nothing can be extrapolated only with these particular values. So, a stability test, with voltages between 26 and 32 V, was conducted as seen in figure 11.



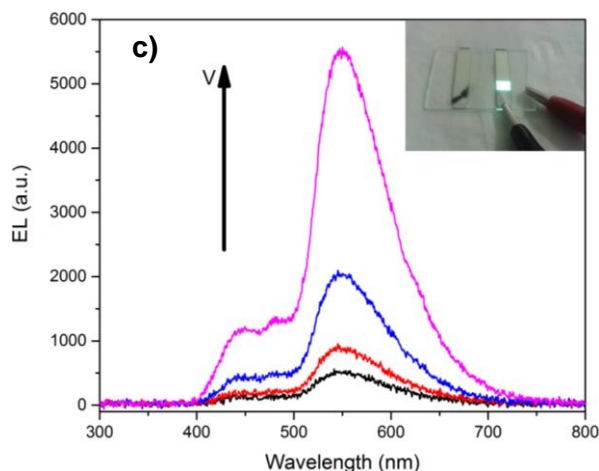


**Figure 11** - a), b), c) EL spectra for the tunable W-OLED i.e. for the devices composed with different concentration of DCM1 I1, I2 and I3 respectively. The inset on each graph shows a picture of the different device at 32 V for a naked eye interpretation. The applied voltages were 26, 28, 30 and 32 V for all samples.

Table 5 shows the translated effects of the devices in terms of color coordinates. These values have a significantly high level of stability, given the low shift in color coordinates when different voltages are applied. The biggest shift is 0.010 which is undetectable by the human eye in the same color region. These results come after supposedly all traps (both natural NPB traps – Chapter I, section 1.2.2. – and energy levels of the dyes) quickly being filled, not contributing to big changes in the color coordinates hence increasing the stability. The quick saturation of traps can be attributed to the use of low level of dyes' concentration.

**Table 5** – Color coordinates for devices I1, I2 and I3 at voltages between 26 and 32 V corresponding to the EL spectra shown in figure 3.

Sample	Voltage (V)	CIE <sub>x</sub>	diff	CIE <sub>y</sub>	diff
I1	26	0.225	-----	0.325	-----
	28	0.231	+0.006	0.315	-0.010
	30	0.238	+0.007	0.314	-0.001
	32	0.238	0	0.317	+0.003
I2	26	0.295	-----	0.422	-----
	28	0.291	-0.004	0.399	-0.003
	30	0.296	+0.005	0.393	-0.006
	32	0.297	+0.001	0.389	-0.004
I3	26	0.372	-----	0.501	-----
	28	0.377	+0.005	0.498	-0.004
	30	0.372	-0.005	0.490	-0.002
	32	0.375	+0.003	0.484	-0.006

### 2.3. Photophysical and energy level analysis: operation theory

Taken into account the results in terms of color tuning and stability, the dynamics inside the blend must be understood in order to effectively allow for an improvement of the whole blend. In fact, the choice of DCM1 arose because this is a typical red emitting dye, used for enhanced luminance in red emitting devices [46] with emissions above 600 nm while C153 was chosen because it is a green

emitting dye [47] with its main emission around 500 nm, according to the supplier. Upon studying the EL spectra from figure 9, the main emission of DCM1 peaks at around 550 nm, i.e. green-yellow emission and C153 appears to be absent or blue-shifted.

To understand this behavior, a Photoluminescence (PL) analysis was conducted to each material, independently – figure 12. DCM1 shows a large emission at around 700 nm, C153 at around 510 nm, both different from what is seen in the EL, while NPB emits at around 450 nm this in accordance with what is seen in the EL. So either the main dyes' emission is blue-shifted or there's an interaction between the materials' energy levels allowing for higher energy transitions. Prior to this work, a similar device but with an active layer of NPB:1%DCM1 was studied. [48] while a device with an active layer of NPB:1%C153 was built. Comparing these results to the EL spectra from figure 9, two things can be concluded:

- When only NPB:C153 is considered, C153 peaks at around 490 nm, compared with the 500 nm expected. Although this difference is low, it can be ascribed to material interaction between the materials for a higher energy emission.
- The main emission spectrum (figure 9) shows similar shape to the NPB:1%DCM1 based device indicating that C153 is not playing a role in the overall emission for the warm white I3. Also, one of the major drawbacks of this device was the relative instable emission with the applied potential, contrary to the ones obtained, meaning that C153 plays an important role of stabilizing the entire matrix.
- The peak at around 490 nm is the result of a blue-shift of the emission of NPB's shoulder at around 510 nm enhanced by the blue-shift emission of C153 (figure 13) since a spectral overlap between C153's PL peak and NPB's shoulder can be seen. An increase of the emission at 490 nm is observed when DCM1's concentration is decreased (I1's cool white and I2's barrier limit white).

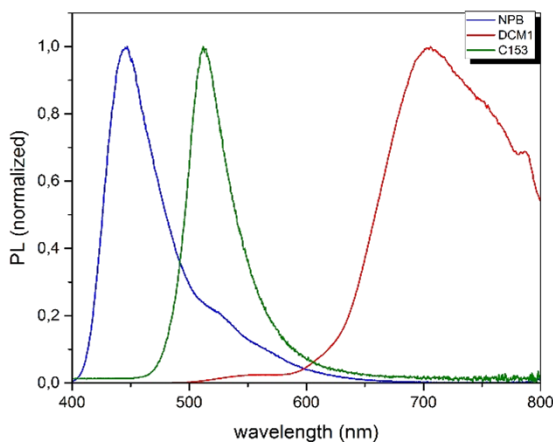


**Figure 12** – Normalized PL spectra of NPB, C153 and DCM1 independently.

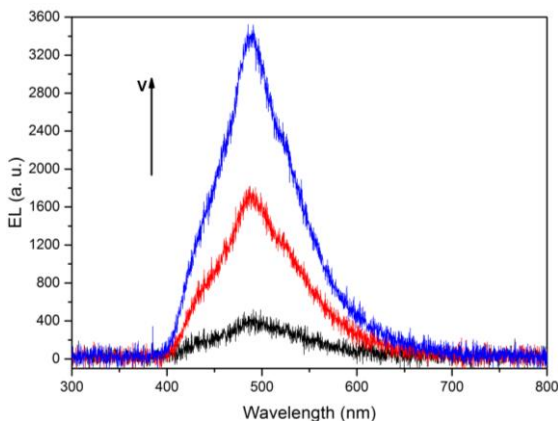


**Figure 13** – EL spectra for a device with an active layer of NPB:1%C153 showing a slight blue-shift of C153’s main emission.

This proves that, for higher DCM1 concentrations, C153 channels carriers from NPB to DCM1 resulting in the stability of the color coordinates. Also, increasing DCM1 allows for more carriers to be channeled resulting in a redshift of the emission peak as shown in figure 9.

Having all this information, a theory regarding the whole device operation can be proposed. Figure 14 shows the energy levels of all materials for a more efficient analysis about the device operation. The LUMO levels of both dyes are below NPB’s, which allows for an easy trapping of electrons, first from NPB to C153 and after to DCM1, all three HOMO levels are in similar energy levels meaning that holes can easily hop between them.

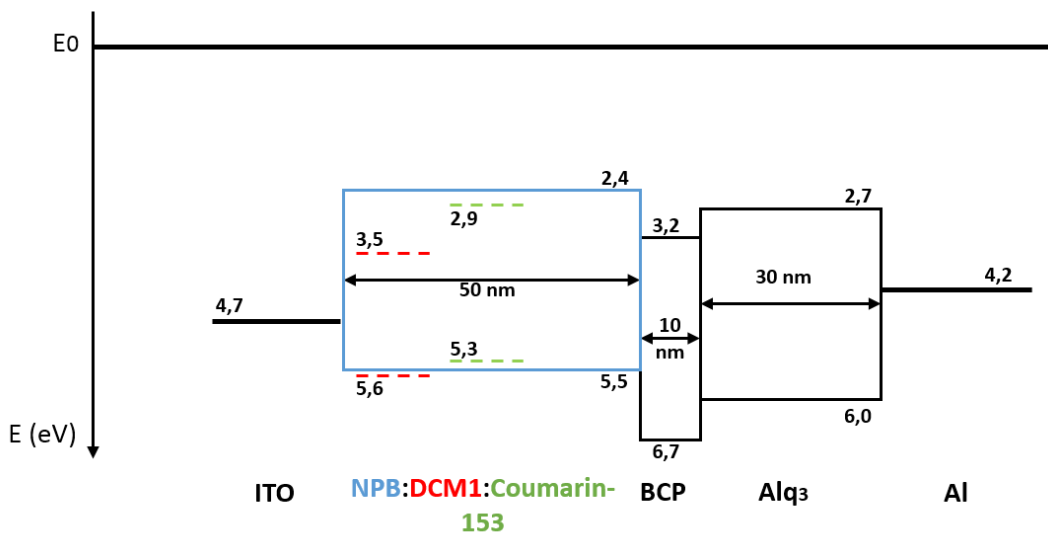


**Figure 14** – Energy levels of all layers constituent of the devices (table 1).

Figure 15 shows all the steps that result in the main emission seen in figure 9 for the proposed theory following a carrier trapping behavior as described in chapter I, section 2.1. If the probability of electrons falling directly from the electrodes into the LUMO levels of both DCM1 and C153 is low, an indirect transition to the dyes through non-radiative transitions is expected. Considering first the interaction NPB-DCM1 (figure 15a), electrons fall from NPB’s LUMO into the excited levels of DCM1. Here, the probability of radiative transition is higher than the non-radiative to lower excited levels



resulting in the emission through them – at higher energies – and not through its LUMO. Raising its concentration, there's an increase of electrons hopping to DCM1, promoting radiative transitions of its lower excited levels, hence the redshift in the emission. Considering C153 (figure 15b), it serves as a facilitator of electron transition, allowing electrons to hop easier to DCM1, stabilizing the emission i.e. allowing for the energy levels of DCM1 to saturate more rapidly (the use of low concentrations allows to do so) and so, the device stability is achieved. C153's non-radiative transition has higher probability over the radiative one at this blend configuration. At low DCM1 concentrations (figure 15c), C153's emission is promoted similarly to DCM1's (emission of the excited levels instead of its LUMO) as a result of the decrease of the amount of electrons that transit in a non-radiative way to DCM1.

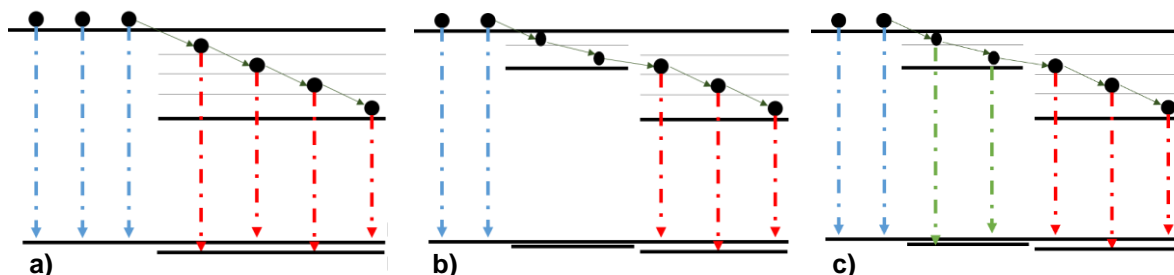


**Figure 15** – Active layer operation. When electrons are injected, they channel to DCM1 in a non-radiative way without C153 (a) or when C153 is added (b) resulting in the emission of light through DCM1. When its concentration is decreased, the emission of C153 (c) is promoted resulted in the increase of the correspondent peak.

This electrostatic nature of the electrons, or the result of the electric field application for the saturation of dopants, appears to have a more significant importance in the device operation opposite to the energy transfer mechanisms. Either there's no spectral overlap between the absorption of the dyes and the emission of NPB, or if there is, it is somewhat irrelevant to the emission. Finally, the Förster transition cannot be excluded though given the low dopant concentration which results in a distance between molecules far above the Förster distance, it is possible to assume that is negligible. A Photoluminescent Excitation (PLE) spectrum would allow for a bigger understanding on this entire behavior and, though it was conducted, the results were inconclusive. The same analysis could also be done in solution but the bathochromic shift would mislead the final result. [49]

### 3. Optoelectronic Characterization

The optoelectronic characterization offers details regarding the viability of an OLED for its general application. It shows how the device operates over its entire regime, its values of brightness and gives great insight on device efficiency, providing information on how to proceed in improving such devices. In this matter, the JVL curves were taken from the set of devices – figure 16.

Though similar in structure, devices I1, I2 and I3 show relative differences in terms of electro-optical behavior. Device I3 (warm white) shows the best results in terms of current density and brightness maximum with  $250 \text{ A/m}^2$  and  $160 \text{ Cd/m}^2$  respectively. This can be a result of the increase of DCM1 with its emission promoted, increasing its brightness value. Although the maximum brightness was relatively lower, it is still in the same order of magnitude when compared to the work

done prior to this project. [48] Similarly, I1 (cool white) appears next ( $J \sim 325 \text{ A/m}^2$  and  $L \sim 120 \text{ Cd/m}^2$ ) where the less efficient emission increase of C153 and general decrease of the emission of DCM1 may be the main responsible for these values. I2 (barrier limit white) has the worst values of the three. The main explanation falls exactly between the other two. This is a barrier limit, both the emissions of C153 and DCM1 are not being promoted in order to produce the color required. Here, the non-radiative transitions appears to be more competitive for such concentrations. These devices could not be compared to other reports in the literature due to the non-use of an integrating sphere (which would show how much light is being emitted from all angles) though a measurement was conducted using the same equipment on an LED monitor. The luminance value obtained was  $180 \text{ Cd/m}^2$  which is close to the 160 obtained for I3. Also, for all kind of devices, it is not possible to confirm if the molecules all evaporated in the same way, even though the conditions were similar which means that, structurally they can be somewhat different (resulting in a different electrical interaction in the EML having, therefore a direct effect on the device operation).

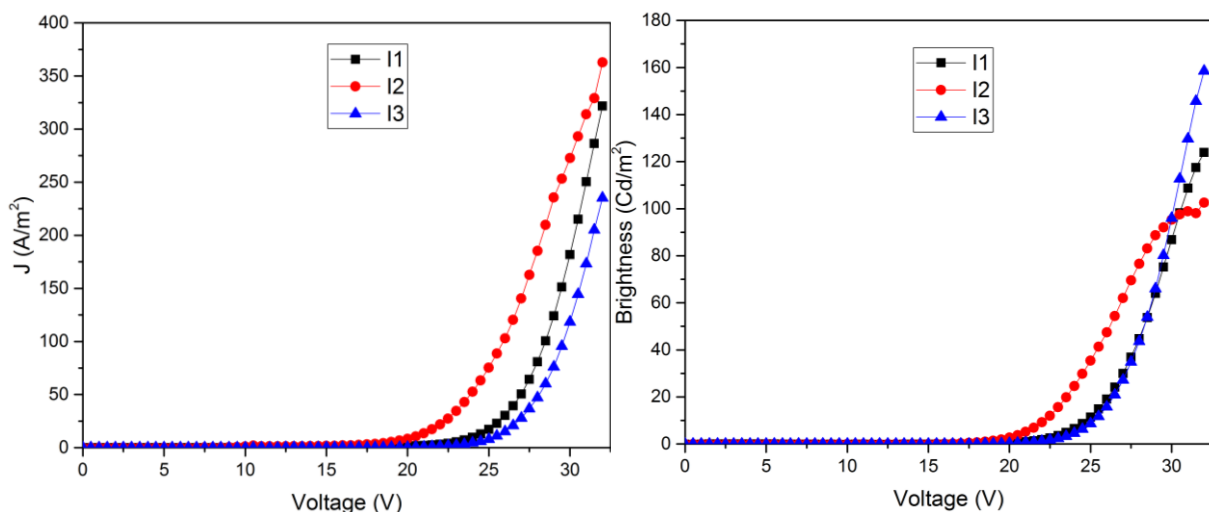


**Figure 16** – JVL curves for devices I1, I2 and I3. The Luminance was taken without background light to reduce ambient effects.

In terms of applied voltages, though devices I1 and I3 start emitting<sup>1</sup> at around 20 V, I2 starts at around 17 V, which may confirm the theory that the structural deposition and/or electrical carrier dynamics throughout Host:Guest may have had an important role here. All devices were put to a limit voltage to understand their behavior. For I2 this resulted in a saturation regime at around 27 V for around  $100 \text{ cd/m}^2$  while I1 and I3 didn't show saturation, giving the relative high threshold voltages.

All devices start operating at a significantly high voltage. Of course, when general lighting is concerned, these values must be reduced, but care must be taken because this is not an optimized structure (it was not the objective of this work) so a further study must be conducted to improve carrier injection and decrease the operating voltage. Also, the resistivity of the ITO film is extremely important

<sup>1</sup> Although it is commonly accepted that EL starts when the device falls in the SCLC region, there must a suitable electron-hole density in order to detect a measurable EL.

for the injection of holes and, in this case, the ITO films had relatively high resistivity values (30-60  $\Omega/\text{sq}$ ) having a direct effect in the threshold voltage.

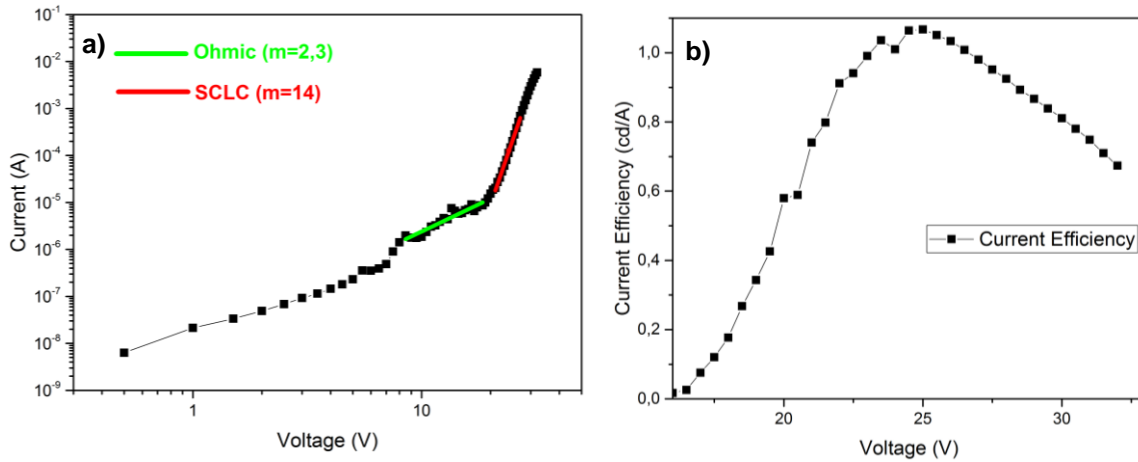


**Figure 17** – a)  $\log(I/V)$  curves for the device I3 displaying the ohmic and SCLC regions. The curve's slope is an evidence of a deep *trap* behavior ( $m > 2$ ). b) Efficiency dependence with voltage of device I3 for an OLED with emission area of  $25 \text{ mm}^2$ .

From the JVL curves, it is possible to gather information regarding the trapping dynamics (section 1.2.2.) – figure 17a. Here, only device I3 was considered giving the previously presented results. Right below the operating voltage, current increases linearly, typical of an ohmic behavior where a small contribution of injected carriers is visible ( $m \sim 2$ ). Upon entering SCLC, i.e.  $V_{\Omega} \sim 12 \text{ V}$ , the slope of 14 ( $> 2$ ) is clear evidence of a deep-trap behavior which follows the proposed theory. Given that the device requires such high applied voltages, the value of  $V_{\text{TFL}}$  could not be determined since it disrupts before hitting it.

Finally, the JVL curves can also give a better understanding on the viability of the operating mechanisms, i.e. the device efficiency  $\eta_{LV}$  (equation 4.1) – figure 17b.

$$\eta_{LV} = \frac{L}{J} = \frac{LA}{I} \quad (4.1)$$

where A is the area. From this data, assuming an emissive area,  $A = 25 \text{ mm}^2$  (figure 8-h), the biggest efficiency obtained was  $1.1 \text{ cd/A}$  for  $25 \text{ V}$  ( $J = 11.17 \text{ A/m}^2$ ), a low value when compared to other devices (Chapter I section 1.3.). The main difference comes from: 1 - the theoretical 25% efficiency in harvesting the singlet excitons, 2 – only the emission at normal angle was considered (no integration was performed) and 3 - the non-optimized structure of the device. This optimization can include:

- Thickness studies meaning how well a layer's thickness can improve the injection/blockage/transport of carriers. [50]
- Plasma treatment of the ITO substrate for work function control. [51]

- Cathode replacement. Studies showed that the use of Calcium<sup>2</sup> passivated with a thin layer of Al can improve the electrode's ability to inject electrons to the organic layers given its reasonably low work function. [3]
- Addition of injection layers such as PEDOT:PSS and/or Lithium Fluoride for holes and electrons, respectively that would increase the charge injection. [52]
- A stepwise structure for the carriers to provide a pathway with low energy barriers between the electrodes and the organic layers. [53]

Still, this value is closer to other reports at a lower complexity and without integration [28], [45], [54] and actually higher than the ones obtained for the same structure without C153. [48] Though this was not the focus of this project, one thing to have in mind when improving it is the need to find a trade-off between the thickness of the device, the correspondent electric field (which will have a direct effect on the charge mobility) and the device's complexit accordingly to its main application. To see the I1 and I2's trapping dynamics and efficiency values, please consult appendix 4.

#### 4. a.c. analysis

##### 4.1. Impedance Spectroscopy (IS)

With the aid of IS (appendix 5) one, in principle, can construct the equivalent circuits and thereby obtain more insights about the operation of the materials, interfaces and devices. At 0 V dc, the device is typically in its ohmic regime so figure 18a shows the Capacitance and the Dielectric loss dependence with frequency.

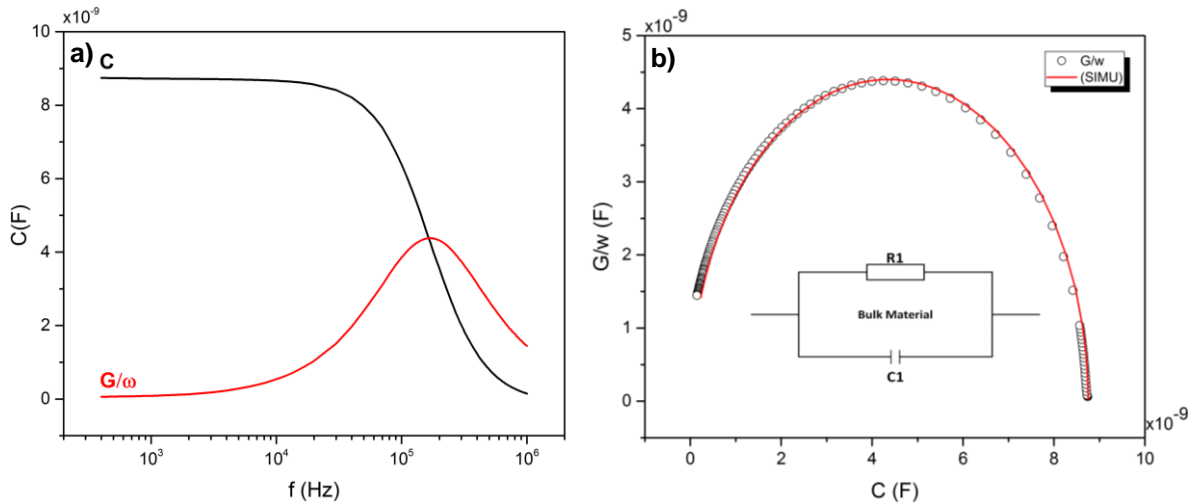


**Figure 18** - a) Capacitance and dielectric loss curves for the device at 0 V dc typical for the ohmic regime. b) Cole-Cole plot, i.e. the dielectric loss as a function of the capacitance for the same device. Following a model described in the inset with a parallel RC for  $R1=110 \Omega$  and  $C1=8.75 \text{ nF}$ , a simulated curve was drawn showing a good fitting can be obtained for this model.

<sup>2</sup> Calcium is extremely sensitive to environment so it needs to be encapsulated prior to the characterization.

From this data, the Cole-Cole plot, which depicts the imaginary part of the impedance (i.e.  $\text{Im}(Z)$ ) or the dielectric loss versus the real part of the impedance (i.e.  $\text{Re}(Z)$ ) or the capacitance when continuously sweeping the small signal frequency (under a particular dc bias) plot, can be extrapolated. The single semicircle shown in figure 18b is typical of an EL single-layer system which, at 0 V dc, is expected given that charge is being accumulated between the electrodes (appendix 5, figure 33a). Joining this with only one relaxation, this kind of behavior is typical of a parallel RC where the resistance describes the conductance of the layer while the capacitor is related to both the layer's thickness and displacement current. This model usually includes a series resistance attached to the parallel RC, typically related to the resistance of the ITO film but, given the tendency of the  $G/w$  to 0 at low frequencies, this is negligible. With the equations described for this model - 5.11 and 5.12 from appendix 5 – for low frequencies, the Capacitance value tends to its geometrical value (equation 5.26), in this case 8.75 nF. Fitting the results with these expressions, the values  $R_1$  and  $C_1$  of 110  $\Omega$  and 8.75 nF respectively, are obtained and the simulated curve clearly shows the overlapping with the obtained values, meaning that this model can be correctly applied for this device. The relaxation frequency, given by the simplification shown in equation 5.21 from appendix 5, is around 165 kHz.

The devices produced here followed a simple principle – that by using a HBL to block carriers in the EML, the emission (or the radiative transitions) would happen solely in this specific layer. IS can aid on the effectiveness of BCP as a whole blocking layer when emission is taking place. So, when entering in the SCLC, this behavior is expected to change. Holes are being accumulated in the HTL/HBL interface (appendix 5, figure 33b) and recombined with the electrons coming from the cathode. The whole dynamic of the device changes with this interfacial behavior and for that, the model must be modified. Figure 19a shows the Capacitance and the Dielectric loss dependence with frequency for the device at 20 V dc, the SCLC regime (figures 16 and 17).

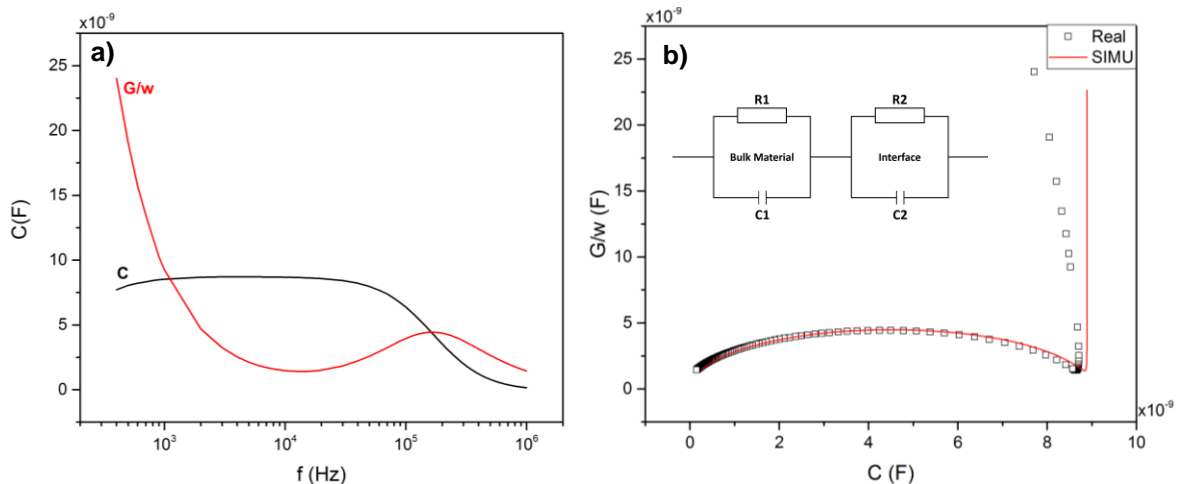


**Figure 19** – a) Capacitance and dielectric loss curves for the device at 20 V dc to assure the SCLC showing interfacial changes in the capacitance dielectric loss values b) Cole-Cole plot, i.e. the dielectric loss as a function of the capacitance for the same device. Following a model described in the inset with a two sets of parallel RC in series for  $R_1=17500 \Omega$ ,  $R_2=105 \Omega$ ,  $C_1=9 \text{ nF}$  and  $C_2=0.02 \text{ nF}$  a simulated curve was drawn showing a good fitting can be obtained for this model. The equipment interference at low frequency results in a deviation of the obtained values.

The results show that there is an interfacial behavior when entering SCLC which is typical with the charge accumulation in the HTL. Two relaxations can be seen at low and high frequencies, respectively. The observed IS data is the result of more than one RC circuit which depend on each other. The model to be applied here should resemble the one shown in the inset of the Cole-Cole plot from figure 19b where it is seen both the interfacial and the bulk dependences. Assuming that, if the frequency tends to 0 Hz (given by the simplification of equation 5.13 from the appendix 5), the Capacitance value tends again to its geometrical value. The values of  $R_1=17.5$  k $\Omega$ ,  $R_2= 105$   $\Omega$ ,  $C_1=9$  nF and  $C_2=20$  pF allow for a good fitting to the obtained results. The discrepancy observed in the Cole-Cole plot at very low frequencies can be ascribed, in a first hypothesis, to typical equipment fluctuations measurements although another physical process cannot be excluded meaning that another model could be applied. Clearly, the carrier trapping inside the HTL governs the OLED behavior and changes in this layer thickness must allow further color modulation.

#### 4.2. Capacitance-Voltage

Given the differences shown between figure 18 and 19 for different applied voltages, the device showed different behaviors in terms of capacitance. To further understand this behavior, the capacitance values from -1.4 to 22 V were measured – figure 20.

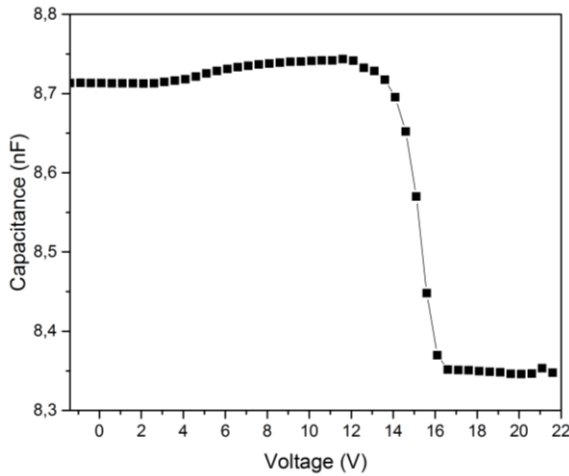


**Figure 20** – Capacitance-voltage measurements of the device shown in figures 9 and 10 at a fixed frequency of 1000 Hz.

So, from equation 5.26 and assuming a thickness  $d_1 = d_{Blend} + d_{Alq_3} + d_{BCP} = 90$  nm,  $\epsilon_r$  of 3.3 (a typical value for organic materials and similar between them [55]) and the emissive area of  $0.25$  cm<sup>2</sup>, the geometrical value of  $C_{geo1} = \frac{\epsilon_r \epsilon_0 A}{d_1} = 8.11$  nF is obtained, which is similar to the 8.71 nF the device shows at low voltages (i.e. ohmic region). When increasing the applied voltage, the capacitance value should increase to the geometric value considering only Alq<sub>3</sub> and BCP as the bulk,  $C_{geo2} = \frac{\epsilon_r \epsilon_0 A}{d_2}$  with a thickness  $d_2 = d_{Alq_3} + d_{BCP} = 40$  nm, of 18.3 nF as holes are accumulated in the HBL/HTL interface. The reason why this isn't happening may well be the same reason to why the high voltages are required for the device to operate – the non-optimized electrodes interfaces. It seems that the voltage required to inject holes into the blend

is closer to the one necessary for electrons to cross the p-type layers, hence the capacitance values. Still, the threshold voltage  $V_t$ , of 3.1 V, seen by the slight increase of the capacitance shows that, though in a small number, some holes are effectively being injected. Finally, the built-in potential,  $V_{bi}$  of 11.6 V given by the small peak of 8.74 nF indicates the transition from ohmic to SCLC and the recombination starts happening, decreasing the capacitance values. This value goes according to what is seen on figure 17a where there's some carrier density injected during operation. Also, by optimizing the structure as described in section 3 of this chapter, the curve may present a behavior similar to the one expected (appendix 5.2 has a complete analysis of a typical CV curve).

### 4.3. Aging Studies

The understanding of the aging mechanism of the organic layers is an important step towards the fundamental dynamics happening inside each device. It usually results in the loss of device performance which includes its luminance and subsequently, efficiency. After evaporation, all devices were left non-encapsulated and exposed to the air (stress conditions), facilitating reactions with ambient gases such as oxygen, which leads to oxygenation of the organic layers and rupture of the entire device. IS can help understand these chemical aging mechanisms as its effects on the capacitance values and relaxation frequencies,  $f_r$ , can be studied.

In this matter, the capacitance and dielectric curves were taken right after its evaporation and with a 24 hour step for three days, with the device being kept on ambient air to promote this aging. Figure 21a shows these curves at 0 V dc

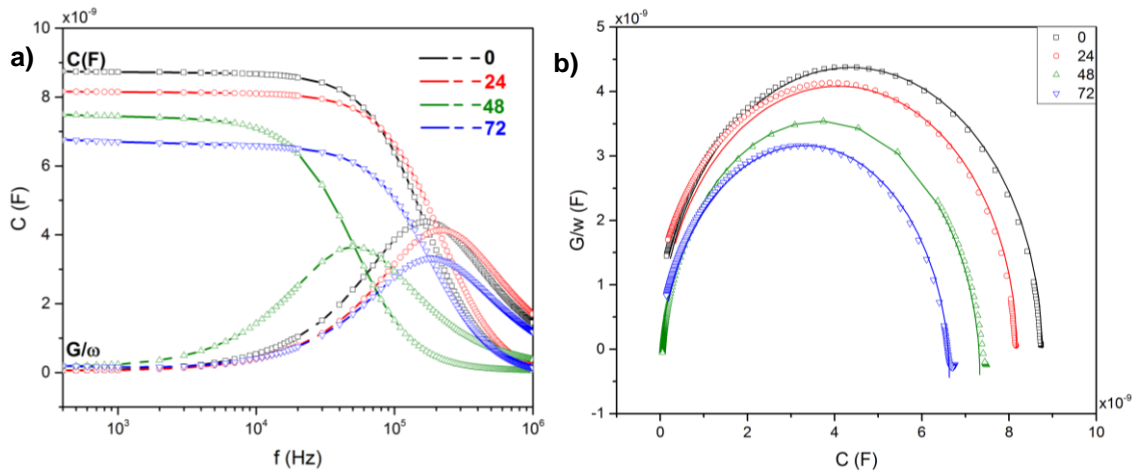


**Figure 21** – a) Capacitance and dielectric loss for the same device at 0 V dc after 0, 24, 48 and 72h at room temperature and ambient air. b) Correspondent Cole-Cole plots overlapped with its simulated curves using the  $R_1$  and  $C_1$  values of table 6 always assuming a parallel RC model.

There is a capacitance drop between measurements that can be attributed to degradation of the Alq<sub>3</sub>/Al interface allowing electrons to move closer to the recombination zone. This confirms a deficiency in charge accumulation resulting in the decrease of the capacitance. Also, a shift in the  $f_r$  to lower frequencies as a result of the increase in the HTL resistance was expected [56] and, though this is generally true (if we assume that the relaxation frequency for 0 and 24h is more or less the same), the data from 72h show reversible changes as  $f_r$  appears to increase from the value for 48h.

From the Cole-Cole plot from figure 21b, assuming the model remains unchanged, the values for R1 and C1 are extrapolated (table 6 confirming the capacitance drop and the overall resistance increase).

**Table 6** – Simulated C1 and R1 with calculated relaxation frequency for the device characterized on figure 21 after 0, 24, 48 and 72h.

Time (h)	C1 (nF)	R1 ( $\Omega$ )	$f_r$ (kHz)
0	8.75	110	165
24	8.17	93	209
48	7.33	425	51
72	6.63	140	171

For the SCLC regime results are shown in figure 22.

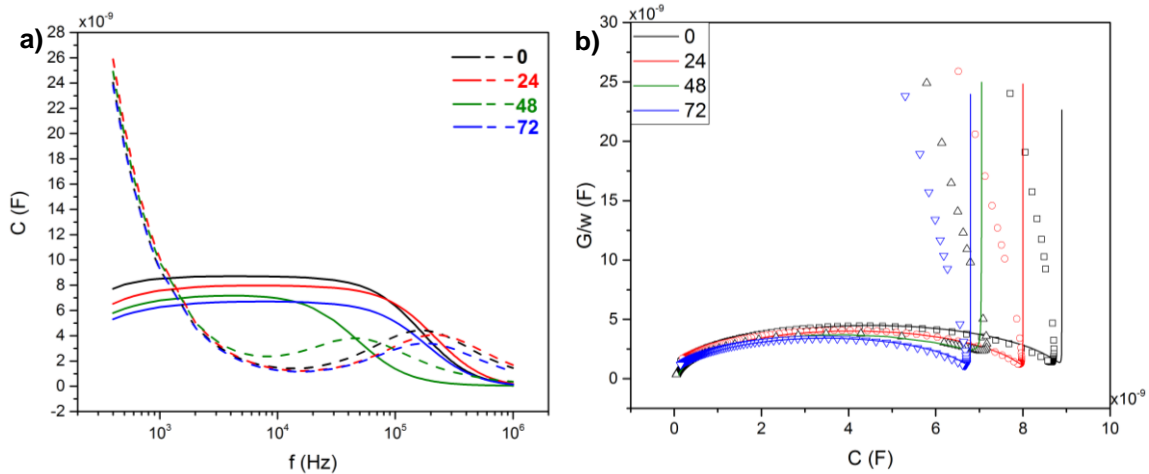


**Figure 22** – a) Capacitance and dielectric loss for the same device at 20 V dc after 0, 24, 48 and 72h on room temperature and ambient air. b) Correspondent Cole-Cole plots overlapped with its simulated curves using the R1, R2, C1 and C2 values of table 7 always assuming a model with a series of two parallel RC.

In a similar way found in the ohmic model, changes after 48 h are observed. As this behavior is similar in both situations, a consideration must be done to ascribe it to an intrinsic physical phenomena. One possible explanation is a different reorganization at a molecular level that appears at this aging level. After that, the expected aging behavior proceeds similarly with the 0 V dc.

**Table 7** – Simulated C1, R1, C2 and R2 with calculated relaxation frequency,  $f_{r1}$  and  $f_{r2}$ , for the device characterized on figure 19 after 0, 24, 48 and 72h.

Time (h)	C1 (nF)	R1 ( $\Omega$ )	C2 (nF)	R2 (k $\Omega$ )	$f_{r1}$ (kHz)	$f_{r2}$ (MHz)
0	9.0	105	0.02	17.50	6.35	476
24	8.1	100	0.06	15.95	7.74	167
48	7.5	485	0.09	15.50	8.60	229
72	6.9	125	0.06	16.50	8.78	133

## 5. Large Area

A SSL device must efficiently emit light on a broad number of substrates which includes emission through flat large area panels. One of the most interesting characteristics of OLEDs is that they offer the same luminous flux of lower luminous intensity by simply expanding the emission area. Some of



these main issues related with increasing the emission area are discussed in appendix 6 which basically include non-uniform light emission, hot spot, power loss, and heat generation. Some of these issues may be overcome with an optimized thermal evaporation system that provides uniform organic films. [57]

As a proof of concept, the emission through larger areas was attempted using a thermal evaporator capable of depositing organic films for emissions larger than the 0.25 cm<sup>2</sup> used so far. Until here (with the Criolab evaporation system), there was no control on the evaporation temperature but on the applied power instead. The evaporation rate was controlled by changing the voltage applied in the crucible so the temperature was high enough to evaporate all materials (considering only the blend). For the large area system (Kurt J. Lesker), when only the blend is concerned and to secure a trade-off between the materials used for deposition and the thickness needed, the evaporation temperature was controlled. All materials have different melting points (table 1) implicating that the temperature needed to be set in order to achieve the desired thickness and concentrations. Having this point optimized, the structure was kept unchanged, the devices were built on a low resistivity ITO film (4-8 Ω/sq from Delta Technologies) and the first concentration attempted was similar to the ones used for I3 (table 3) for a warm white source. The results are described in figure 23.

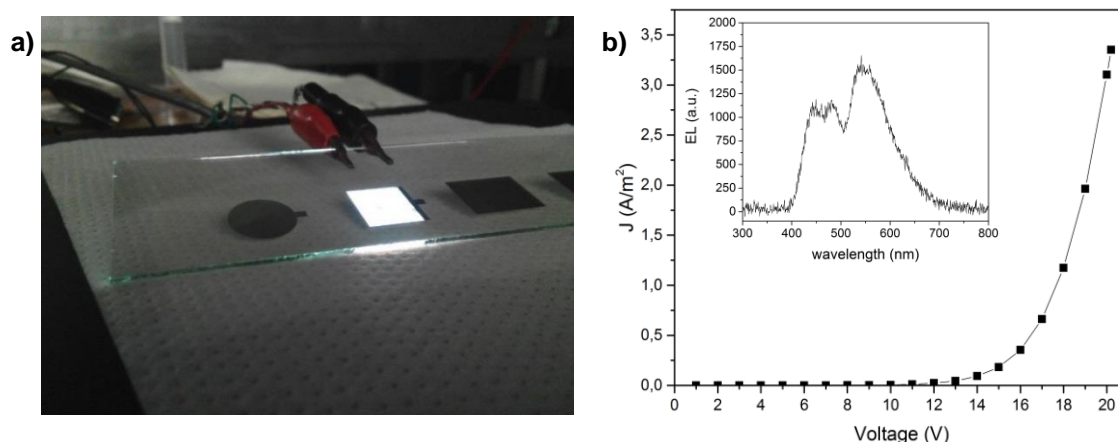


**Figure 23** – a) barrier limit OLED with an active layer of 2.25 cm<sup>2</sup>. b) JV curve for the device in figure 23a. The use of a low resistivity ITO film decreased the threshold voltage to around 11 V. Inset shows the EL spectra for a typical barrier limit white emission. This barrier white emission was obtained for concentrations of 98.3%:1%:1 of NPB:C153:DCM1 respectively.

An increase in the active area of 9 times to 2.25 cm<sup>2</sup> – figure 23a was achieved. This device showed a broad, stable emission even with increased area. The current density and the threshold voltage both decreased as a result of the increase in the emission area and the use of a low resistivity ITO film. The inset in figure 23b suggests a behavior typical of a barrier limit white emission (I2 – figure 9) which implies that, when increasing the emission area and changing the ITO resistivity, the temperature control implies a tuning in the concentrations for each equipment, as a result of the different melting points of the blended materials.

The broad emission of this device proved it was possible to increase the emission area even further and so, figure 24 shows the typical cool white light (for an attempted barrier limit white – table 2) on a 16 cm<sup>2</sup> emission area, i.e. an increase of 64 times of the first area attempted. The level of defects – specially non-emissive areas – start to become visible as seen in figure 24a, which may appear during the cleaning or the evaporation processes as these become even more relevant for a stable emission. One of the advantages of the use of OLEDs is the broad emission through all directions and can be clearly seen in the lateral side of figure 24a.

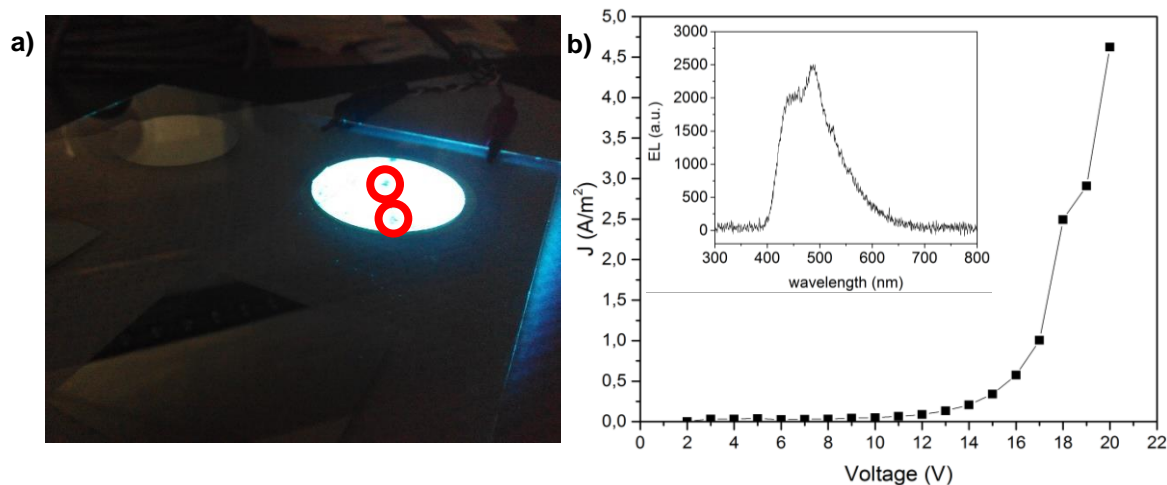


**Figure 24** – a) cool white OLED with an active layer of 16cm<sup>2</sup> and highlighted defects. b) JV curve for the device in figure 24a with threshold voltage of around 11 V. Inset shows the EL spectra for a cool white emission with a low emission from DCM1 which may be the result of a low material evaporation. Increasing this should increase the amount of DCM1 in the final evaporated blend. This cool white emission was obtained for concentrations of 98.3%:1%:0.7 of NPB:C153:DCM1 respectively.

Even though this adjustment was necessary, the final result is still quite satisfying because 1) this limit still remains low and 2) the physical models proposed for low emission area (chapter IV, section 2.2.) are being confirmed. The increase of the emission area was effectively achieved. It showed that this is still a work in progress as the main emission shows some level of defects. As the main objective was the scale-up, this serves as a proof of concept of the applicability for a SSL device. The next step includes the optimization of the films' production to secure a uniformity between layers which, for example, includes the optimization of the patterning of the ITO film. The final device produced had a different patterning technique where the anode area did not contact the tape used. This resulted in the emission shown in figure 25 where the number of non-emissive areas decreased. So the main proof of concept is achieved as these devices can be applied for general lighting sources. As a curiosity, the maximum luminance (75 cd/m<sup>2</sup>) and the efficiency (0.7 cd/A) were also taken showing a decrease in these values which are a result of the increased area (increased area results in the decrease of the luminance - [58]). The final considerations in terms of optimization includes an encapsulation process to avoid ambient problems as seen before. Finally, once this is secured, the device optimization explained in section 3, part IV can be included for operation voltage reduction.

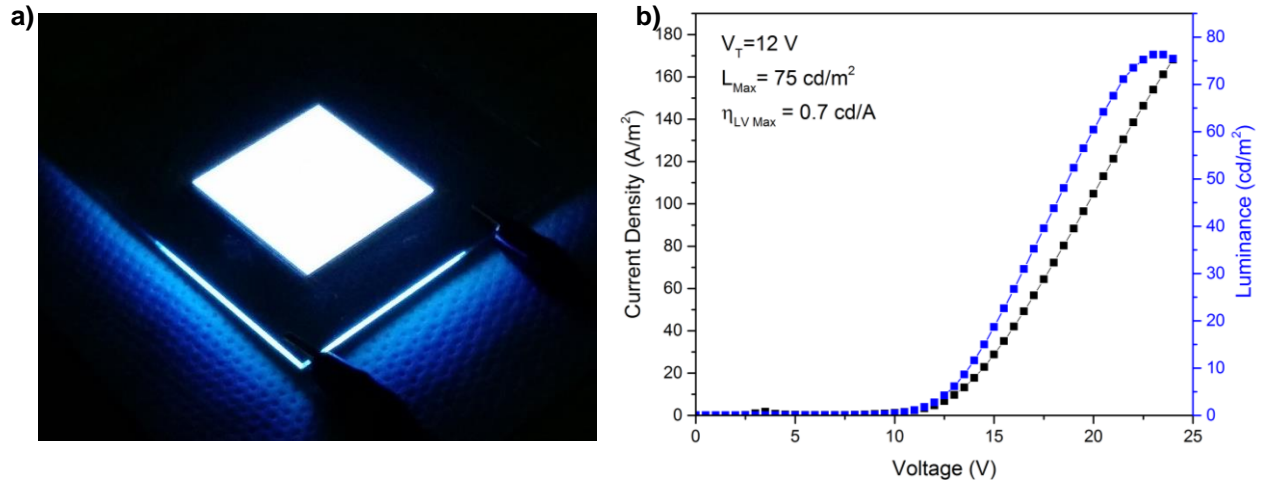


**Figure 25** – a) cool white OLED with an active layer of  $16\text{cm}^2$  produced with an optimized ITO patterning. b) JVL characteristic for this device showing a voltage drop for the threshold voltage as a result of a decrease in the ITO's resistivity.



## Chapter V: Conclusion and future trends

---

Color tunable White Organic Light Emitting Diodes (W-OLEDs) based on a single emitting layer composed with NPB (blue host), Coumarin-153 (green guest) and DCM1 (red guest) for a host:guest RGB emission, were successfully produced. By changing DCM1's concentration from 0.5% to 1% and keeping C153's at 1%, the final color, shown in the Electroluminescence (EL) spectra and translated in changes in the figures of merit of the corresponding devices, could be tuned from cool to warm white. This EL behavior of the blend was attributed to the interaction between NPB and the dopant dyes. While DCM1 was extremely important in the color tuning process, C153 behaved as a carrier channel and as a stabilizer of the overall emission. The final device configuration was ITO/Blend/BCP/Alq<sub>3</sub>/Al where BCP was chosen as Hole Blocking Layer and Alq<sub>3</sub> as an Electron Transport Layer and, given the emission through the blend, this proves that they are both behaving efficiently. As a proof of concept, this same structure was applied in large area panels which allowed for an increase of 9 and 64 times the first initial area attempted. This specific part showed that an optimization study is critical for the broad emission of the device.

The optoelectronic characterization showed that, although high operating voltages were seen, luminance as high as 160 cd/m<sup>2</sup> was achieved together with device efficiencies up to 1.1 cd/A. These values are comparable with the ones obtained for similar experimental conditions. The high operating voltages can be, in first approximation, addressed to the high resistivity ITO films (which have a significant effect on the hole injection) and/or the non-optimized electrodes-organic layer interfaces. In terms of operating behaviors, the device showed a typical Space Charge Limited Current (SCLC) beginning at around 12 V, while it started emitting at around 20 V with a deep trap kind of behavior. This was expected given that the energy levels of the dopants, especially the Least Unoccupied Molecular Orbital (LUMO), fall deep compared to NPB's.

Though the devices were reproducible, the non-control of the evaporation temperature, which could have an influence in the concentration of the final blended films deposited, could present some difficulties when applying this structure to other evaporation systems. Still, as it was shown by the large area devices, this was only translated in slight adjustments in the blend's fine tuning for each evaporation equipment. A co-evaporation could also be considered but, given the low concentrations used for DCM1 and C153, it can't be applied.

The Impedance Spectroscopy (IS) analysis conducted showed that the device can be modelled with simple sets of parallel RC circuits, not only in the ohmic but also in the SCLC regions. The Cole-Cole plot of this last one suggests the appearance of a second relaxation for lower frequencies that must be proved by conducting the same analysis for frequencies below 100 Hz. IS was also used as an aging probe study which was translated in both the reduction of capacitance (in fact related to the loss of charge retaining ability in the Alq<sub>3</sub>/Al interface) and general increase in resistance (which lowers the relaxation frequency) for both regimes.

It is the first time this color tuning ability, allied with high stability, low level of complexity and large area emission is reported. This, of course with the main application for general lighting in mind. Also, it used 100% commercially available materials for the device structure. None of them were lab synthesized specifically for this project which increases, even more, the device's simplicity. Comparing this set of results with other light sources available (appendix 2.2.), this may offer a wider range of color tunes with the same, if not higher, values of Color Rendering Index (CRI). In this matter, OLEDs for general lighting may be a sustainable solution to the ever increasing scarcity problem. Also, considering the effects that artificial lighting can have in the human body, these different tunes can help simulate the natural daylight while also improving productivity, discussed more extensively in the motivation where the effects of lighting in the biologic cycle is considered.

In terms of future perspectives, there is a lot that needs to be done to effectively produce a commercially interesting Solid State Lighting (SSL) device. First, the introduction of another red dye could red-shift the color coordinates resulting in, for example, more faithful warm white devices. Red Nile can be a good candidate giving its emission on late-red, infrared wavelengths and suitable HOMO-LUMO levels [59]. Because the operating voltage was high and the efficiency quite low, an optimization study must be conducted. This optimization can come from lowering the ITO's resistivity or even replacement, changing the overall device thickness, or improve the injection of carriers by introducing injection layers which would decrease the amount of carriers accumulated between the electrodes. In this matter, keeping the complexity level low is extremely important, so there must be a trade-off between the device efficiency and its complexity to decrease the production costs. All of this implies, of course, optimized evaporating systems to decrease the levels of defects shown in the large area panels. The increase of the area proved a great advantage but work must still be done to increase it even further. This can include an adaptation of the cleaning process and the evaporation system itself. Finally, two important aspects must be taken into account for future work. First, considering that all the materials used are soluble, the device can be built in wet-deposition systems such as Roll-to-roll (R2R), decreasing, even more, the device production costs if a mass production is expected. Second, given the applicability of this structure, a flexible Polyethylene substrate can be used as an application for flexible organic electronics.

## References

- [1] A. Jägerbrand, "New Framework of Sustainable Indicators for Outdoor LED (Light Emitting Diodes) Lighting and SSL (Solid State Lighting)," *Sustainability*, vol. 7, no. 1, pp. 1028–1063, 2015.
- [2] V. K. Khanna, *Fundamentals of Solid-State Lighting*, 1st ed., no. 518. Press, CRC, 2014.
- [3] N. Thejokalyani and S. J. Dhoble, "Organic light emitting diodes: Energy saving lighting technology - A review," *Renew. Sustain. Energy Rev.*, vol. 16, no. 5, pp. 2696–2723, Jun. 2012.
- [4] J. F. Duffy and C. a. Czeisler, "Effect of Light on Human Circadian Physiology," *Sleep Med. Clin.*, vol. 4, no. 2, pp. 165–177, 2009.
- [5] L. Schlangen, "Circle of light The effect of light on our sleep/wake cycle principal scientist at Philips Executive summary," *Philips*, 2014.
- [6] C. W. Tang and S. a. Vanslyke, "Organic electroluminescent diodes," *Appl. Phys. Lett.*, vol. 51, no. 1987, pp. 913–915, 1987.
- [7] J. H. Burroughes, D. D. C. Bradley, a. R. Brown, R. N. Marks, K. Mackay, R. H. Friend, P. L. Burns, and a. B. Holmes, "Light-emitting diodes based on conjugated polymers," *Nature*, vol. 347, p. 539, 1990.
- [8] S. Reineke, M. Thomschke, B. Lüssem, and K. Leo, "White organic light-emitting diodes: Status and perspective," *Rev. Mod. Phys.*, vol. 85, no. 3, pp. 1245–1293, Jul. 2013.
- [9] R. H. Friend, R. H. Friend, R. W. Gymer, R. W. Gymer, a. B. Holmes, J. H. Burroughes, a. B. Holmes, J. H. Burroughes, R. N. Marks, C. Taliani, R. N. Marks, D. D. C. Bradley, C. Taliani, D. D. C. Bradley, D. a. Dos Santos, M. Lo, J. L. Bredas, M. Logdlund, W. R. Salaneck, W. R. Salaneck, D. a. Dos Santos, J. L. Bre, and V. Slyke, "Electroluminescence in conjugated polymers," *Nature*, vol. 397, pp. 121–128, 1999.
- [10] Y. Zhang and S. R. Forrest, "Triplets contribute to both an increase and loss in fluorescent yield in organic light emitting diodes," *Phys. Rev. Lett.*, vol. 108, no. June, pp. 1–5, 2012.
- [11] L. Pereira, "The Organic-LED Basics," in *Organic Light Emitting Diodes: The Use of Rare Earth and Transition Metals*, 1st ed., Singapore: Pan Stanford Publishing, 2011, pp. 11–22.
- [12] S. Schols, *Device Architecture and Materials for Organic Light-Emitting Devices - Targeting High Current Densities and Control of the Triplet Concentration*, 1st ed. Springer, 2011.
- [13] L. Pereira, "Bulk Carrier Transport: Hopping," in *Organic Light Emitting Diodes: The Use of*

*Rare Earth and Transition Metals*, 1st ed., Singapore: Pan Stanford Publishing, 2011, pp. 64–66.

- [14] V. M. Silva and L. Pereira, “The nature of the electrical conduction and light emitting efficiency in organic semiconductors layers: The case of [m-MTDATA] - [NPB] - Alq3 OLED,” *J. Non. Cryst. Solids*, vol. 352, pp. 5429–5436, 2006.
- [15] Dongge Ma and I. A. H. ummelgen, “Charge Carrier Mobility and Electroluminescence in a Green-Emitting Alternating Block Copolymer with a Methoxy Bi-Substituted Chromophore,” *Brazilian J. Phys.*, vol. 30, no. 2, pp. 392–397, 2000.
- [16] M. Mart, “Charge Transport in Organic Semiconductors With Application To,” 2010.
- [17] L. Pereira, “Injection Limit: The Schottky Barrier at Electrode– Semiconductor Interface,” in *Organic Light Emitting Diodes: The Use of Rare Earth and Transition Metals*, 1st ed., Singapore: Pan Stanford Publishing, 2011, pp. 46–53.
- [18] V. K. Khanna, “Understanding Lighting Processes from Luminescence Theory,” in *Fundamentals of Solid-State Lighting*, 1st ed., Press, CRC, 2004, pp. 65–67.
- [19] A. Köhler and H. Bässler, “From Orbitals to States,” in *Electronic Processes in Organic Semiconductors*, 1st ed., Wiley-VCH, Ed. Singapore, 2015, pp. 25–31.
- [20] B. C. Krummacher, V.-E. Choong, M. K. Mathai, S. a. Choulis, F. So, F. Jermann, T. Fiedler, and M. Zachau, “Highly efficient white organic light-emitting diode,” *Appl. Phys. Lett.*, vol. 88, no. 11, p. 113506, 2006.
- [21] J.-H. Jou, S. Kumar, A. Agrawal, T.-H. Li, and S. Sahoo, “Approaches for fabricating high efficiency organic light emitting diodes,” *J. Mater. Chem. C*, 2015.
- [22] J. Kido, M. Kimura, and K. Nagai, “Multilayer white light-emitting organic electroluminescent device,” *Science*, vol. 267, no. March, pp. 1332–1334, 1995.
- [23] P. E. Burrows, S. R. Forrest, S. P. Sibley, and M. E. Thompson, “Color-tunable organic light-emitting devices,” *Appl. Phys. Lett.*, vol. 69, no. 20, p. 2959, 1996.
- [24] C. L. Lin, T. Y. Cho, C. H. Chang, and C. C. Wu, “Enhancing light outcoupling of organic light-emitting devices by locating emitters around the second antinode of the reflective metal electrode,” *Appl. Phys. Lett.*, vol. 88, no. 2006, pp. 111–114, 2006.
- [25] J. Liu, “Pure white OLED based on an organic small molecule: 2,6-Di(1H-benzo[d]imidazol-2-yl)pyridine,” *Spectrochim. Acta Part A Mol. Biomol. Spectrosc.*, vol. 149, pp. 48–53, 2015.
- [26] V. Gohri, S. Hofmann, S. Reineke, T. Rosenow, M. Thomschke, M. Levichkova, B. Lüssem, and K. Leo, “White top-emitting organic light-emitting diodes employing a heterostructure of down-conversion layers,” *Org. Electron. physics, Mater. Appl.*, vol. 12, no. 12, pp. 2126–2130,



2011.

- [27] T. Schwab, M. Thomschke, S. Hofmann, M. Furno, K. Leo, and B. Lüssem, "Efficiency enhancement of top-emitting organic light-emitting diodes using conversion dyes," *J. Appl. Phys.*, vol. 110, no. 8, p. 083118, 2011.
- [28] a. Uddin, C. B. Lee, and J. Wong, "Emission properties of dopants rubrene and coumarin 6 in Alq3 films," *J. Lumin.*, vol. 131, no. 5, pp. 1037–1041, 2011.
- [29] B. W. D'Andrade and S. R. Forrest, "White organic light-emitting devices for solid-state lighting," *Adv. Mater.*, vol. 16, no. 18, pp. 1585–1595, 2004.
- [30] W. S. Jeon, T. J. Park, S. Y. Kim, R. Pode, J. Jang, and J. H. Kwon, "Ideal host and guest system in phosphorescent OLEDs," *Org. Electron. physics, Mater. Appl.*, vol. 10, no. 2, pp. 240–246, 2009.
- [31] A. Köhler and H. Bässler, "Förster and Dexter Type Energy Transfer," in *Electronic Processes in Organic Semiconductors*, 1st ed., Singapore: Wiley-VCH, 2015, pp. 119–123.
- [32] T. Forster, "10th Spiers Memorial Lecture. Transfer mechanisms of electronic excitation," *Discuss. Faraday Soc.*, vol. 27, no. 10, p. 7, 1959.
- [33] A. Misra, P. Kumar, M. N. Kamalasanan, and S. Chandra, "White organic LEDs and their recent advancements," *Semicond. Sci. Technol.*, vol. 21, no. 7, pp. R35–R47, 2006.
- [34] S. Chen, Q. Wu, M. Kong, X. Zhao, Z. Yu, P. Jia, and W. Huang, "On the origin of the shift in color in white organic light-emitting diodes," *J. Mater. Chem. C*, vol. 1, p. 3508, 2013.
- [35] X. Zhang, Z. Wu, B. Jiao, D. Wang, D. Wang, X. Hou, and W. Huang, "Solution-processed white organic light-emitting diodes with mixed-host structures," *J. Lumin.*, vol. 132, no. 3, pp. 697–701, 2012.
- [36] L. Pereira, "Methods for Processing Organic Semiconductors," in *Organic Light Emitting Diodes: The Use of Rare Earth and Transition Metals*, 1st ed., Singapore: Pan Stanford Publishing, 2011, pp. 33–36.
- [37] S. H. Kim, J. Jang, and J. Y. Lee, "High efficiency phosphorescent organic light-emitting diodes using carbazole-type triplet exciton blocking layer," *Appl. Phys. Lett.*, vol. 90, no. 2007, pp. 1–4, 2007.
- [38] Sigma-Aldrich, "NPB (N,N'-Di(1-naphthyl)-N,N'-diphenyl-(1,1'-biphenyl)-4,4'-diamine)." ref:556696.
- [39] M. a. Baldo, S. Lamansky, P. E. Burrows, M. E. Thompson, and S. R. Forrest, "Very high-efficiency green organic light-emitting devices based on electrophosphorescence," *Appl. Phys. Lett.*, vol. 75, no. 1, pp. 4–6, 1999.

- [40] Sigma-Aldrich, "BCP (Bathocuproine)." ref:699152.
- [41] Sigma-Aldrich, "Alq3 (Tris-(8-hydroxyquinoline)aluminum)." ref:444561.
- [42] G. Zhong, K. Kim, D. W. Lee, and J. Il Jin, "Photoluminescent and electroluminescent properties of DCM-1 dispersed poly(p-phenylene vinylene) derivatives," *Synth. Met.*, vol. 156, no. 9–10, pp. 731–735, 2006.
- [43] Sigma-Aldrich, "DCM1(4-(Dicyanomethylene)-2-methyl-6-(4-dimethylaminostyryl)-4H-pyran)." ref:410497.
- [44] Sigma-Aldrich, "Coumarin-153." ref:546186.
- [45] V. K. Rai, R. Srivastava, and M. N. Kamalasanan, "White organic light-emitting diodes based on blue fluorescent bis(2-(2-hydroxyphenyl)benzoxazolone)zinc [Zn(hpb)<sub>2</sub>] doped with DCM dye," *Synth. Met.*, vol. 159, pp. 234–237, 2009.
- [46] C.-T. Chen, "Evolution of Red Organic Light-Emitting Diodes: Materials and Devices," *Chem. Mater.*, vol. 16, no. 23, pp. 4389–4400, 2004.
- [47] M. L. G. Horng, Ja Papazyan, a Maroncelli, M, "Subpicosecond Measurements of Polar Solvation Dynamics - Coumarin-153 Revisited," *J. Phys. Chem.*, vol. 99, no. 48, p. 17337, 1995.
- [48] J. Costa, "Fabrico e caracterização de W-OLEDs em substrato rígido e flexível João Miguel Marreiro Costa Fabrico e caracterização de W-OLEDs em substrato rígido e flexível," 2013.
- [49] V. Bulović, R. Deshpande, M. . Thompson, and S. . Forrest, "Tuning the color emission of thin film molecular organic light emitting devices by the solid state solvation effect," *Chem. Phys. Lett.*, vol. 308, no. 3–4, pp. 317–322, 1999.
- [50] S. K. So, W. K. Choi, L. M. Leung, and K. Neyts, "Interference effects in bilayer organic light-emitting diodes," *Appl. Phys. Lett.*, vol. 74, no. 14, p. 1939, 1999.
- [51] H. Park, H. Kim, S. K. Dhungel, J. Yi, S. Y. Sohn, and D. G. Jung, "Impedance Spectroscopy Analysis of Organic Light-Emitting Diodes Fabricated on Plasma-Treated Indium-Tin-Oxide surfaces," *J. Korean Phys. Soc.*, vol. 51, no. 3, p. 1011, 2007.
- [52] L. Ying, C.-L. Ho, H. Wu, Y. Cao, and W.-Y. Wong, "White polymer light-emitting devices for solid-state lighting: materials, devices, and recent progress.," *Adv. Mater.*, vol. 26, p. 2459, 2014.
- [53] J.-H. Jou, Y.-S. Wang, C.-H. Lin, S.-M. Shen, P.-C. Chen, M.-C. Tang, Y. Wei, F.-Y. Tsai, and C.-T. Chen, "Nearly non-roll-off high efficiency fluorescent yellow organic light-emitting

- diodes," *J. Mater. Chem.*, vol. 21, no. 34, p. 12613, 2011.
- [54] W. Chen, L. Lu, and J. Cheng, "Characterization of two-emitter WOLED with no additional blocking layer," *Optik (Stuttg.)*, vol. 121, no. 1, pp. 107–112, 2010.
- [55] W. Brütting, S. Berleb, and A. G. Mückl, "Device physics of organic light-emitting diodes based on molecular materials," *Org. Electron.*, vol. 2, no. 1, pp. 1–36, 2001.
- [56] S. Nowy, W. Ren, a Elschner, W. Lovenich, and W. Brutting, "Impedance spectroscopy as a probe for the degradation of organic light-emitting diodes," *J. Appl. Phys.*, vol. 107, pp. 54501–54509, 2010.
- [57] J. W. Park, "Large-area OLED lighting panels and their applications," in *Organic light-emitting diodes (OLEDs): Materials, devices and applications*, Woodhead Publishing Limited, 2013, pp. 572–608.
- [58] S. Reineke, F. Lindner, G. Schwartz, N. Seidler, K. Walzer, B. Lüssem, and K. Leo, "White organic light-emitting diodes with fluorescent tube efficiency," *Nature*, vol. 459, no. 7244, pp. 234–238, 2009.
- [59] P. Greenspan, E. P. Mayer, and S. D. Fowler, "Nile red: a selective fluorescent stain for intracellular lipid droplets, *J. Cell Biol.* 100 (1985) 965–973.," *J. Cell Biol.*, vol. 100, no. 10, pp. 965–973, 1985.
- [60] N. Thejokalyani and S. J. Dhoble, "Novel approaches for energy efficient solid state lighting by RGB organic light emitting diodes – A review," *Renew. Sustain. Energy Rev.*, vol. 32, pp. 448–467, 2014.
- [61] N. Zheludev, "Commentary. The life and times of the LED - a 100-year history," *Nat. Photonics*, vol. 1, pp. 189–192, 2007.
- [62] H. Johnston, "Isamu Akasaki, Hiroshi Amano and Shuji Nakamura win 2014 Nobel Prize for Physics," *Physics World*, 2014. [Online]. Available: <http://physicsworld.com/cws/article/news/2014/oct/07/isamu-akasaki-hiroshi-amano-and-shuji-nakamura-win-2014-nobel-prize-for-physics>. [Accessed: 09-Mar-2015].
- [63] G. C. M.N. Kamalasanan, Ritu Srivastava and P. T. and A. K. Arunandan Kumar, "Organic Light Emitting Diode," in *Knowledge Creation Diffusion Utilization*, 1st ed., M. Mazzeo, Ed. India: Sciyo, 2010, pp. 183–185.
- [64] S. Nowy, "Understanding losses in OLEDs: optical device simulation and electrical characterization using impedance spectroscopy," 2010.
- [65] D. L. Chinaglia and G. Gozzi, "Espectroscopia de impedancia no laboratorio de ensino," *Rev. Bras. Ensino Fis.*, vol. 30, no. 4, p. 4505, 2008.

- [66] J. W. Park, D. C. Shin, and S. H. Park, "Large-area OLED lightings and their applications," *Semicond. Sci. Technol.*, vol. 26, no. 3, p. 034002, 2011.
- [67] Brooke Jensen, "Dealership LED Lighting: The Brightest Way to Add Value to Your Lot," *Dealers United*, 2015. [Online]. Available: <http://blog.dealersunited.com/sales/dealership-led-lighting-the-brightest-way-to-add-value-to-your-lot>. [Accessed: 09-Sep-2015].

## Appendices

### 1. Solid State Lighting

Artificial lighting is used by mankind since the fire era. From fire to candles, bulb lamps to the current technology, a big evolution has happened. 200 years ago came the first artificial lighting source – the incandescent lamp, where a voltage is typically applied in a tungsten filament allowing it to emit light. Still, though they are the least expensive, they have the lowest efficiency (most of the energy is emitted in the form of heat) and lifetime (1000–2000h of use). Then came the fluorescent lamp, a low-pressure mercury-vapor gas discharge lamp covered with phosphor. When an electric current is applied, it excites the mercury in the tube allowing it to emit Ultraviolet Light (UV) that will further be absorbed by the phosphor resulting in the emission of visible light (around 50 % of the UV emitted is used to promote the emission of the Vis light). They can be 3 to 5 times more efficient than the standard incandescent lamps and last 10 to 20 times longer. Still, they use highly pollutant materials, such as mercury. Compact fluorescent lamps (CFLs) came later with some improvements but still based on a similar principal. [8],[60]

None of these technologies offer an efficient way of producing white light so, later came the need to improve these devices in order to reduce the heat generation and the use of pollutant materials. Solid State Lighting (SSL) came to supplant some of the drawbacks referred before. The working principle of these devices is based on solid state electroluminescence. Light is emitted upon the injection of charge carriers (electrons and holes) into semiconductor materials where they recombine and, from the energy decay of this recombination, comes the emission of light with a wavelength corresponding to the energy of its transition. The first Light Emitting Diode (LED) was reported in 1928. Since then, several advances have been made leading to the current high efficiencies and lifetimes (40000 to 10000h) but some drawbacks remain. Firstly, they require the use of direct-gap semiconductors to allow for the radiative transition. Secondly, they are point light sources having a limited viewing range and lastly, in order to produce white light, they use either a red–blue–green array or a phosphor-coated blue LED which lowers the efficiency. [61] Thus, the development of this field garnered an impressive reputation leading to the Nobel Prize in physics in 2014. [62]

### 2. Color quality of white light sources

For illuminating purposes, a white source must possess a high illumination quality to be applied to general lighting which is translated accordingly to the figures of merit correspondent to each source: the Commission Internationale d'Eclairage (CIE) chromaticity coordinates ( $x,y$ ), the Color Correlated Temperature (CCT) and the Color Rendering Index (CRI).[2] This allows for qualitatively define the color quality of such devices. With this considered, it is possible to address on different color sources and see how efficient they are when lighting is concerned.

#### 2.1. Figures of merit

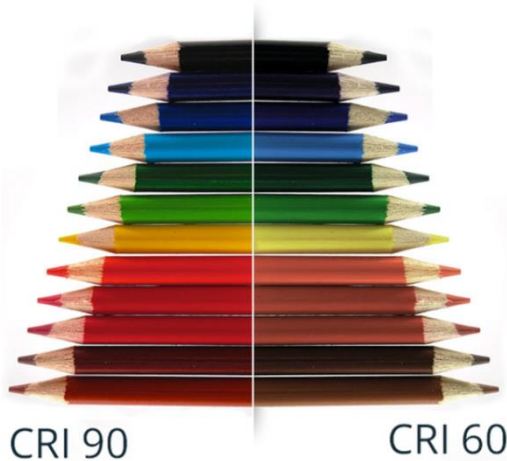
##### a) CIE 1931 ( $x,y$ )



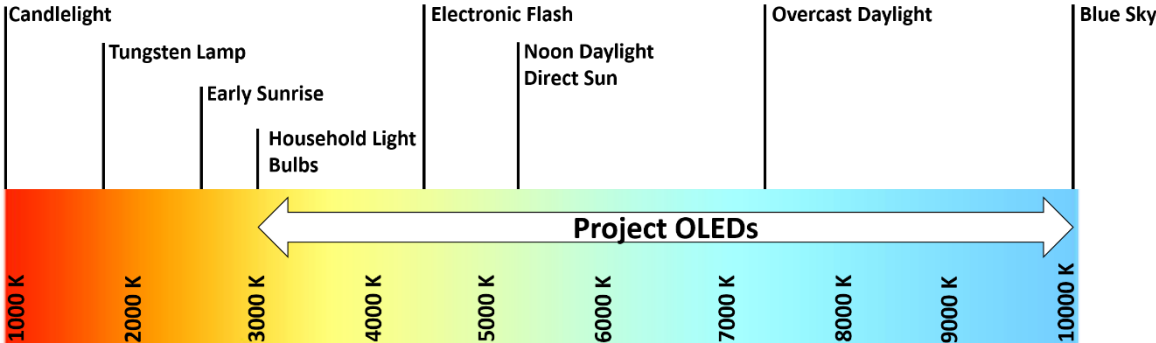
and it is measured in 0-100 scales, with 100 representing true color perfection. A monochromatic light will have a low CRI - an orange lamp, for instance, will only ever render orange colors, whereas a polychromatic light with balanced RGB counterparts will have a high CRI being able to reproduce all different colors from different objects. It is thus important that light sources possess good color rendering so as to ensure that objects appear natural. Illumination-quality white light usually implies a CRI equal or above 80. Figure 27 shows the effects of light sources with different values of CRI clearly showing the main interest in building high CRI devices.

**c) CCT**

True color temperature is the color of radiation emitted from a perfect blackbody radiator<sup>4</sup> held at a particular temperature, being defined in units of Kelvin. The light of an incandescent bulb comes from thermal radiation, being the color temperature associated with the temperature of the filament. Light sources other than incandescent lamps are described in terms of the Color Correlated Temperature, CCT. The CCT is the temperature of a blackbody radiator that has a color that most closely matches the emission from a non-blackbody radiator which can also be obtained with the EL spectrum. For comparison purposes, figure 28 shows typical CCT values for different sources which also includes the range that this project’s OLEDs got.[60]



**Figure 27** – The effects of light sources with high (90) and low (60) Color Rendering Indexes. A high CRI means that a color source effectively covers the entire visible spectrum being able to reproduce all the surrounding colors. Low CRI, on the other hand, may lack Red, Green or Blue counterparts resulting in inefficient reproducibility of the surrounding environment. (adapted from [67])

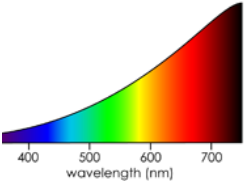
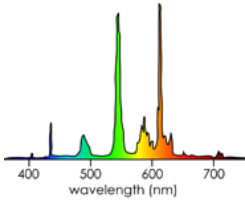
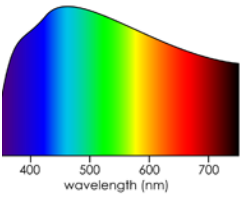
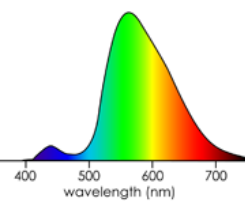
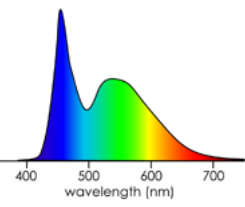
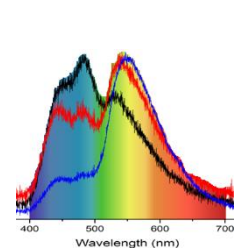


**Figure 28** – CCT values for different sources including range for the produced OLEDs.

<sup>4</sup> A blackbody radiator is a source that is able to emit light with all wavelengths.

## 2.2. Light Sources

**Table 8** – Basic EL spectra of different light sources and corresponding CCT and CRI values for comparison purposes with the result obtained with this project.[63]

		CCT (K)	CRI
Incandescent		~2500	90-95
Fluorescence		~4000	50-90
Daylight		6000	~100
Warm White LED		~3000	70
Cool White LED		~7000	90
Color tunable W-OLED		3200-10500	89-91



### 3. Radiative and Non-Radiative Transitions

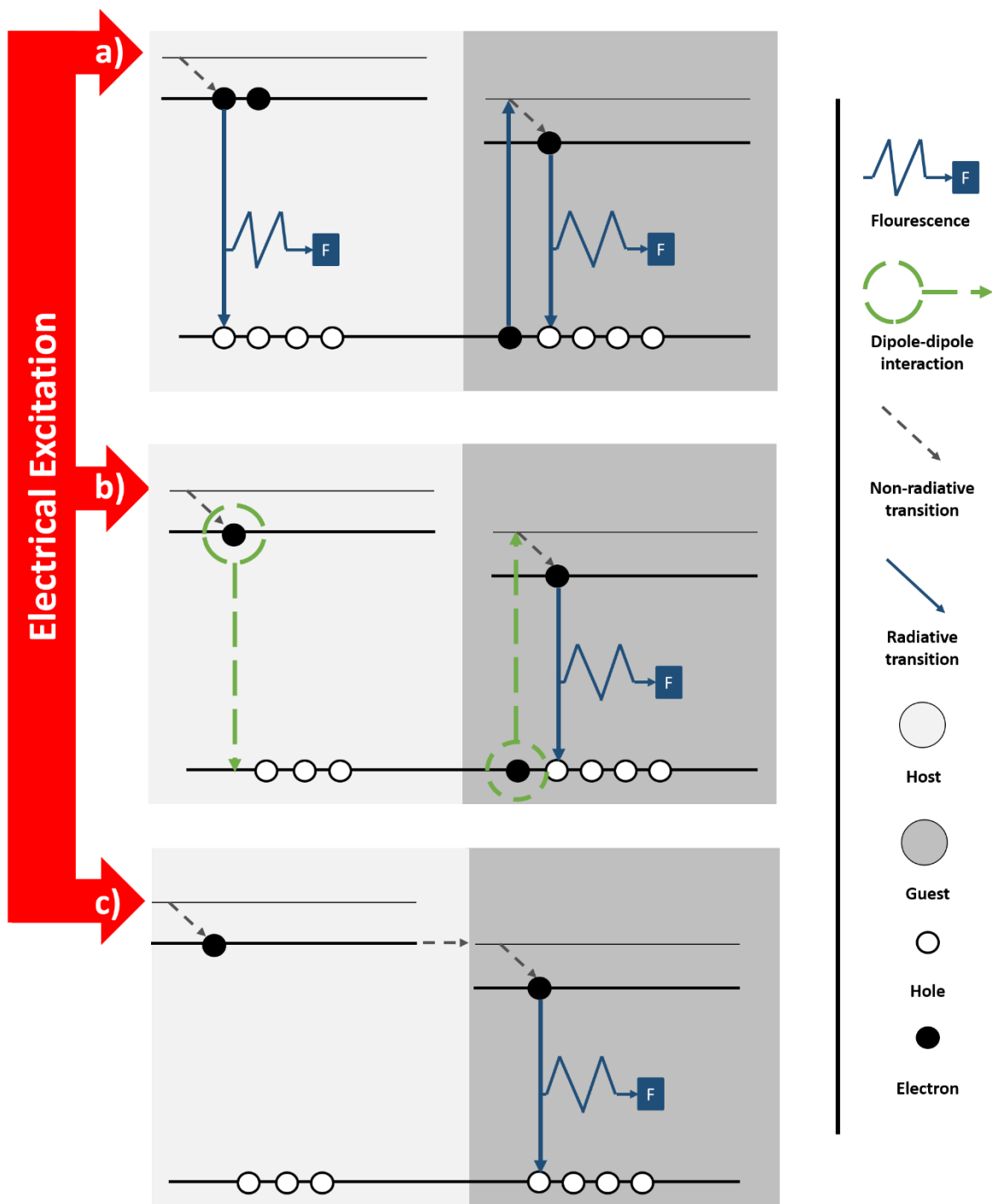


**Figure 29**– Energy transitions in a Host:Guest system (section 2.1.) namely the energy transfer (either through radiative a) and non-radiative i.e. the Förster transition b)) and the carrier trapping c).

#### 4. I1 and I2 Optoelectrical Characterization

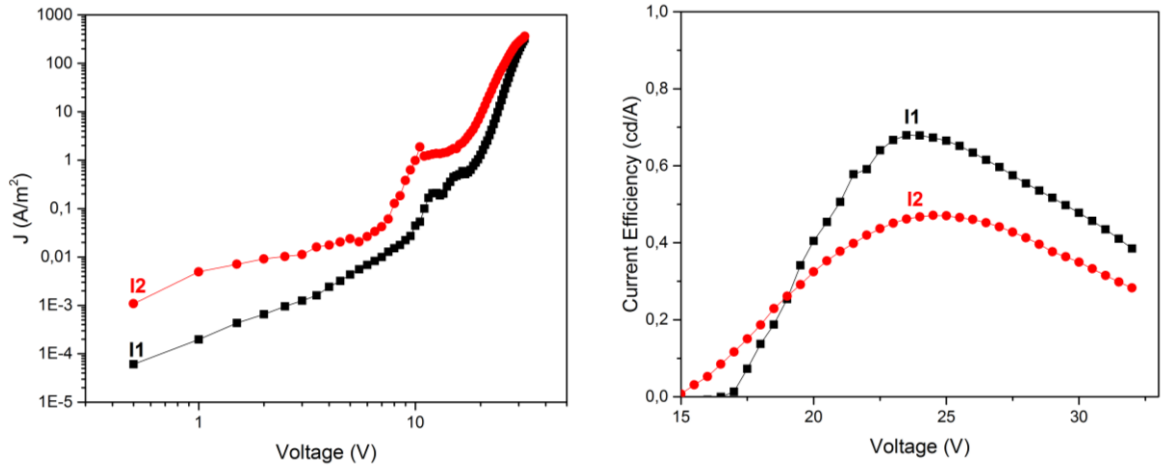


**Figure 30** – a) JV curves and b) current efficiency values for devices I1 and I2.

#### 5. Impedance spectroscopy of OLED

To assess about the electrical behavior of materials or devices, Impedance Spectroscopy (IS) is a great tool since it allows for the understanding of inherent processes inside of them, which includes interfacial (electrode organic or organic-organic) information, such as charge injection, blockage, accumulation and diffusion coefficients. It is based on the appliance of an alternate signal (ac) between two electrodes and measure the real and imaginary parts of the impedance with frequency. With the results obtained, one must compare with a RC model that can correctly describe the device's behavior.

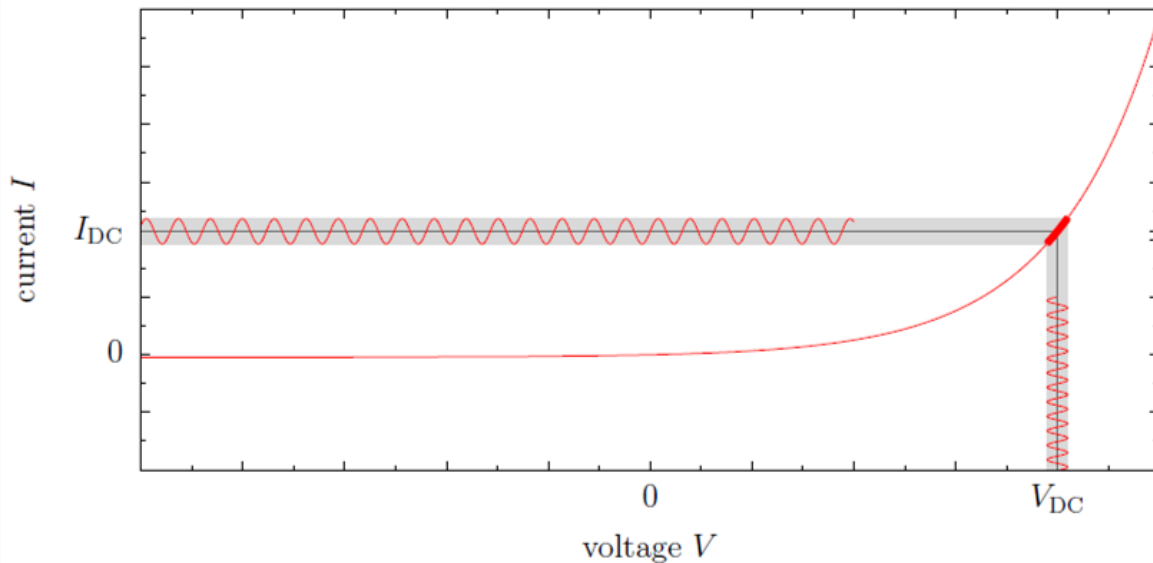


**Figure 31** – IV curve of an ideal diode. For IS measurements, a bias voltage  $V_{DC}$  is chosen followed by the appliance of an alternating signal  $V_{AC}(t)$  and the corresponding  $I_{AC}(t)$  is obtained. [64]

Considering a small alternating signal  $V(t)$  – figure 31 – with and ac counterpart  $V_{AC}(t) = V_{AC} \cdot \cos(2\pi f \cdot t)$  and its response  $I(t)$ :

$$V(t) = V_{DC} + V_{AC}(t) \quad (5.1)$$

$$V(t) = V_{DC} + V_{AC} \cdot \cos(2\pi f \cdot t) \quad (5.2)$$

$$I(t) = I_{DC} + I_{AC} \quad (5.3)$$

$$I_{AC}(t) = I_{DC} + I_{AC} \cdot \cos(2\pi f \cdot t + \varphi) \quad (5.4)$$

where  $\varphi$  is a phase shift between voltage and current. Defining  $\hat{Z}(f)$  as the complex impedance i.e. the ratio of the applied alternating voltage and the current response in complex notation  $\hat{V} = V_{AC} \cdot \exp(i \cdot 2\pi f \cdot t)$  and  $\hat{I} = I_{AC} \cdot \exp(i \cdot (2\pi f \cdot t + \varphi))$  comes:

$$\hat{Z}(f) = \frac{\hat{V}}{\hat{I}} = \frac{V_{AC}}{I_{AC}} \cdot \exp(-i\varphi) = \text{Re}(\hat{Z}) + i \cdot \text{Im}(\hat{Z}) \quad (5.5)$$

$$|\hat{Z}| = \sqrt{\text{Re}^2(\hat{Z}) + \text{Im}^2(\hat{Z})} \quad (5.6)$$

$$\varphi = \arctan \frac{\text{Im}(\hat{Z})}{\text{Re}(\hat{Z})} \quad (5.7)$$

Depending on the measurement equipment used, different equivalent may be used to correctly represent the complex impedance. For semiconductor devices, the capacitance  $C$  and the dielectric loss<sup>5</sup> (the conductance  $G$  divided by the angular frequency  $\omega = 2\pi f$ ) are the most commonly used

$$C(\omega) = \frac{1}{\omega} \cdot \frac{-\text{Im}(\hat{Z})}{\text{Re}^2(\hat{Z}) + \text{Im}^2(\hat{Z})} \quad (5.8)$$

$$\frac{G(\omega)}{\omega} = \frac{1}{\omega} \cdot \frac{\text{Re}(\hat{Z})}{\text{Re}^2(\hat{Z}) + \text{Im}^2(\hat{Z})} \quad (5.9)$$

### 5.1. Equivalent circuits

As explained before, the results obtained can be fitted into a model that correctly describes the device. Because every layer of an organic material has its own conductivity and dielectric constant, the device can be represented by a set of a parallel RC circuit depending on its behavior with the applied signal. The impedance of a parallel RC is described by equation 5.10 and, for the work in question, two circuits are considered (figure 32), both based on this equation. [64], [65]

$$\hat{Z}_{RC} = \frac{1}{\frac{1}{R} + i\omega C} \quad (5.10)$$

<sup>5</sup> Dielectric loss is also defined as the loss of energy (such as heat) when varying the electric field.

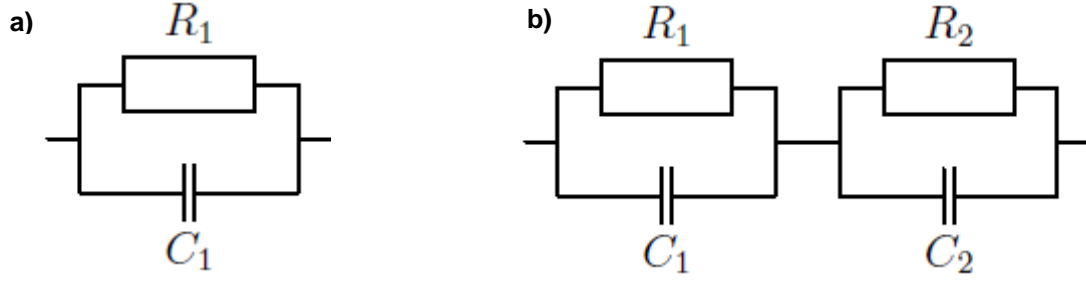


**Figure 32** – Models considered for an IS analysis based on a) single and b) double parallel RC circuits

For circuit 1:

$$\hat{Z} = \hat{Z}_{R_1 C_1} \quad (5.11)$$

$$C(f) = \frac{C_1}{w^2 R_1^2 C_1^2 + 1} \quad (5.11)$$

$$\frac{G(w)}{w} = \frac{w R_1}{w C_1^2 R_1 + 1} \quad (5.12)$$

For circuit 2:

$$\hat{Z} = \hat{Z}_{R_1 C_1} + \hat{Z}_{R_2 C_2} \quad (5.14)$$

$$C(w) = \frac{R_1^2 C_1 + R_2^2 C_2 + w^2 R_1^2 R_2^2 \cdot C_1 C_2 \cdot (C_1 + C_2)}{((R_1 + R_2)^2 + w^2 R_1^2 R_2^2 \cdot C_1 C_2 \cdot (C_1 + C_2)^2)} \quad (5.13)$$

$$\frac{G(w)}{w} = \frac{1}{w} \left[ \frac{R_1 + R_2 + w^2 R_1 R_2 (R_1 C_1^2 + R_2 C_2^2)}{((R_1 + R_2)^2 + w^2 R_1^2 R_2^2 (C_1 + C_2)^2)} \right] \quad (5.14)$$

The relaxation frequency, given by the middle in the general decrease in the capacitance at a specific frequency can be generally described by equations 5.15-5.17. This is the frequency where carriers stop following the applied signal.

$$C(f_r) = C_f + \frac{C_i - C_f}{2} \quad (5.15)$$

$$C_i = \lim_{f \rightarrow 0} C(f) \quad (5.16)$$

$$C_f = \lim_{f \rightarrow \infty} C(f) \quad (5.17)$$

From equation 5.15 the relaxation frequency,  $f_r$  can be determined as a simplification of equation 5.15-5.17 for the corresponding model.

For circuit 1:

$$C_i = C_1 \quad (5.18)$$

$$C_f = 0 \quad (5.19)$$

$$C(f_r) = \frac{C_1}{2} \quad (5.20)$$

$$f_r = \frac{1}{2\pi C_1 R_1} \quad (5.21)$$

For circuit 2:

$$C_i = \frac{(R_1^2 C_1 + R_2^2 C_2)}{(R_1 + R_2)^2} \quad (5.22)$$

$$C_f = \frac{(C_1 C_2)}{C_1 + C_2} \quad (5.23)$$

$$C(f_r) = \frac{1}{2} \frac{(R_1 C_1 + R_2 C_2)}{((R_1 + R_2)^2 (C_1 + C_2)^2)} \quad (5.24)$$

$$f_r = \frac{1}{2\pi R_1 R_2 (C_1 + C_2)} \quad (5.25)$$

## 5.2. Capacitance-Voltage Measurements

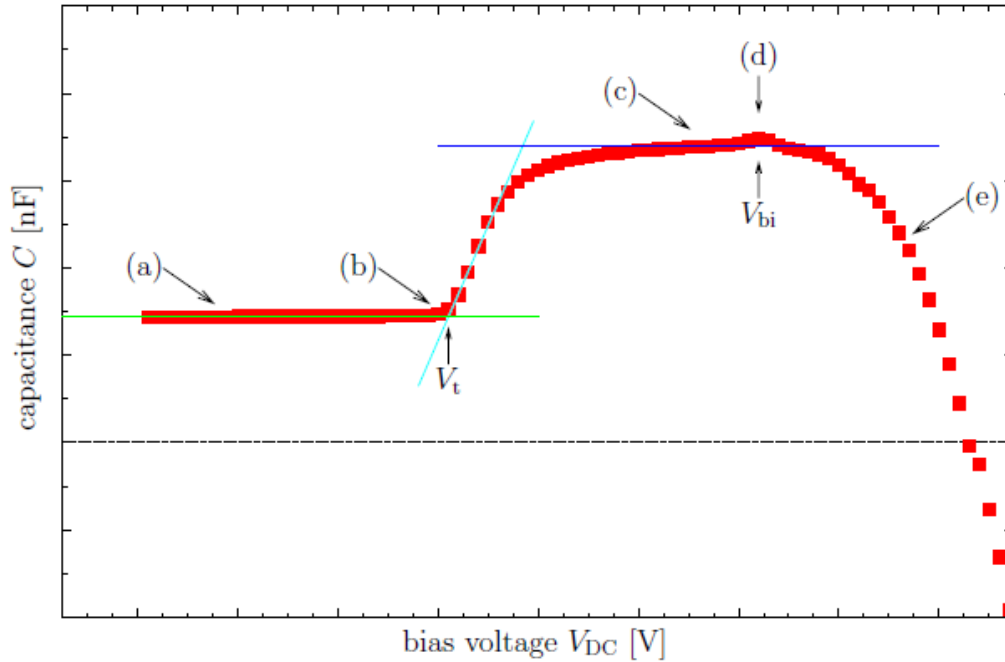


**Figure 33** – CV measurement of an OLED device. The values were left out purposely being of particular interest the behavior and not the constitution of the device (adapted from [64])

Figure 33 shows an example of a Capacitance-Voltage (CV) measurement in an OLED device. Its purpose is to give an insight of some of the inherent characteristics and what to expect when conducting this type of measurement. To ensure this analysis is correctly done, three assumptions must be taken into account:

1. The device is generically structured as Cathode/HTL/ETL/anode with the emission taking place at the HTL;
2. The HTL is less resistive than the ETL meaning charge will be injected easily;
3. The relative permittivity,  $\epsilon_r$ , of the of ETL and HTL is assumed to be the same.

Finally, expression 5.15 gives the geometric capacitance which is important whenever charge is being accumulated in an interface:

$$C_{geo} = \frac{\epsilon_r \epsilon_0 A}{d} \quad (5.26)$$

where  $\epsilon_0$  is the electric constant,  $A$  the area considered and  $d$  the thickness. By analyzing figure 33 it is possible to describe all phases occurring:

- (a)  $V < V_t$  charge is not injected into the device and the value measured corresponds to the geometric capacitance of all the device (figure 34a);
- (b)  $V = V_t$  injection of holes into the anode/HTL interface begins;
- (c)  $V_t < V < V_{bi}$  holes accumulate at the HTL/ETL interface meaning that capacitance will rise to the value of the geometric capacitance of ETL (figure 34b). This comes as a result of the resistivity differences between layers;
- (d)  $V = V_{bi}$  limit applied bias for charge accumulation. Electrons will surpass the value of resistivity and will be able to be injected into the ETL. Once charge reaches the HTL/ETL interface, annihilation of charge will begin, photons will be emitted and charge will decrease;
- (e)  $V > V_{bi}$  charge decreases being able to get negative values, which is common for a bipolar injection;

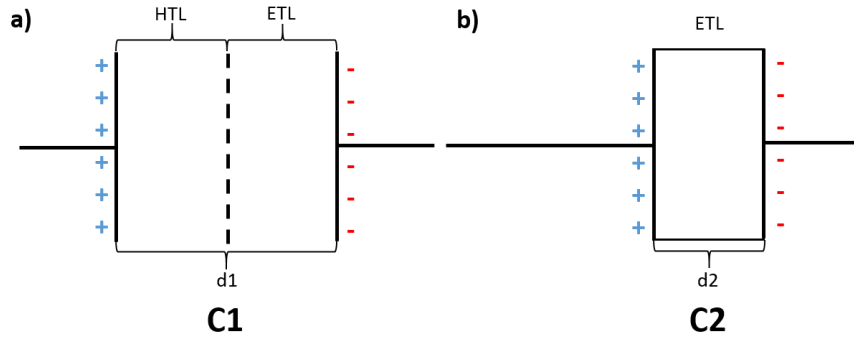


**Figure 34** – geometric capacitance of the device analyzed for a)  $V < V_t$  and b)  $V_t \leq V < V_{bi}$  based on eq. 5.26,  $C_2 > C_1$ .

## 6. Increasing the emission area

One of the major objectives in this project was to increase the emission area while keeping the structure unchanged. This constituted the greatest challenge and the basic proof of concept on whether or not this materials could effectively be applied for SSL devices. The effects of increasing area are briefly discussed in section 5, chapter IV though a more detailed analysis must be done to understand the key issues related to the fabrication of large-area OLEDs. [57], [66]

- a) **Short-Circuit:** unwanted particles on the glass substrate or formed during evaporation may result in a short pathway for current flow and thus the short circuits. These particles can be accumulated as a result of an insufficient cleaning process, misalignment of evaporation masks, vacuum problems (that can result in shadow effects), migration of the cathode through the organic layers, among others. Also, it can arise when an initial bias voltage is applied, or as the bias voltage is varied. More seriously, however, it occurs even during a very stable operation and, though it can be suppressed, it is still a reliability issue. The main solution for this problem comes from the changing on the different layer's thickness which

can include the use of a tandem device structure (with individualized OLEDs on top of each other) without any compromise on the device performance.

- b) Non-uniform light distribution:** this problem is directly related to differences in terms of device thickness in the emissive layer. It has different thicknesses across its layer, the resulting current will also be different by which the light emission distribution becomes non-uniform. Also, non-uniformity can arise from the limiting conductivity of the transparent anode, where the injected current from the edge of a panel hardly reaches its central region. The problem becomes more serious with increasing luminous intensity. It is also induced by a variation of organic films during large-area thermal evaporation. To tackle this problem, one may need to consider the ratio between the effective horizontal resistance of the anode and the vertical resistance of the OLED device to promote an effective carrier path between layers. Again, the tandem structure can be of use though employing a highly conductive metal (Ag) sandwiched between two conductive oxides, or the use of low-resistance auxiliary metal lines to the central region can improve significantly the emission uniformity. The luminance uniformity can also be enhanced by reducing a contact resistance between OLED electrodes and driving boards. The contact area between them is preferred to be large to promote injection from every direction.
- c) Hot Spot:** this is the main cause for the device lifetime as spikes and a rough surface of the transparent anode together with particles result in an increase in current and thus local heat generation.
- d) Efficiency reduction:** the power loss as the resistance of the anode is raised directly affects the power efficiency. This entails various forms of device optimization as discussed throughout this project and include functional layers in the device configuration such as electron and hole blocking layers, interlayers for exciton blocking, etc.
- e) Heat Generation:** as seen in other light sources (see motivation), thermal-related issues are a big problem. With increased area, the device must be prepared to promote efficient heat dissipation – heat sink – to block device degradation. Here, the encapsulation plays an important role here as heat transfers to a heat sink through its encapsulation layers. The typical glass encapsulation has low thermal conductivity resulting in nitrogen accumulation inside the device, separating the organic layers from the heat sink. Thin-film encapsulations, on the other hand, has the best heat dissipation as a result of a short heat transfer pathway.





